Research Square

Preprints are preliminary reports that have not undergone peer review.
They should not be considered conclusive, used to inform clinical practice,
or referenced by the media as validated information.

The class VIII myosin ATM2 stabilizes actin-plasma membrane contacts by locally promoting PtdIns(4,5)P2 nanodomain formation in tobacco pollen tubes

Ingo Heilmann

ingo.heilmann@biochemtech.uni-halle.de

Institute for Biochemistry and Biotechnology, Martin-Luther-University Halle-Wittenberg
https://orcid.org/0000-0002-2324-1849

Vera Wagner

Institute for Biochemistry and Biotechnology, Martin-Luther-University Halle-Wittenberg

Marta Fratini

Institute for Biochemistry and Biotechnology, Martin-Luther-University Halle-Wittenberg
https://orcid.org/0000-0003-0934-3854

Johanna Uhlenberg

Institute for Biochemistry and Biotechnology, Martin-Luther-University Halle-Wittenberg

Alexandra Schutkowski

Institute for Biochemistry and Biotechnology, Martin-Luther-University Halle-Wittenberg

Christoph Kastner

Institute for Biochemistry and Biotechnology, Martin-Luther-University Halle-Wittenberg

Kirsten Bacia

Institute of Chemistry, Martin Luther University Halle-Wittenberg

Article

Keywords: Actin-dynamics, Actin-membrane interface, PIP5K2, Membrane-nanostructure, PIP2

Posted Date: October 7th, 2025

DOI: https://doi.org/10.21203/rs.3.rs-7598484/v1

License: This work is licensed under a Creative Commons Attribution 4.0 International License.
Read Full License

Additional Declarations: There is **NO** Competing Interest.

Title

The class VIII myosin ATM2 stabilizes actin-plasma membrane contacts by locally promoting PtdIns(4,5)P_2 nanodomain formation in tobacco pollen tubes

Authors

Vera Wagner[1], Marta Fratini[1], Johanna Uhlenberg[1], Alexandra Schutkowski[1], Christoph Kastner[1], Kirsten Bacia[2], and Ingo Heilmann[1]

[1] Department of Plant Biochemistry, Institute of Biochemistry and Biotechnology, Martin Luther University Halle-Wittenberg, Halle (Saale), Germany

[2] Department of Biophysical Chemistry, Institute of Chemistry, Martin Luther University Halle-Wittenberg, Halle (Saale), Germany

Short title

ATM2 promotes PtdIns(4,5)P_2-formation

Keywords

Actin-dynamics, Actin-membrane interface, PIP5K2, Membrane-nanostructure, PIP_2

Author for Correspondence

Ingo Heilmann

Department of Plant Biochemistry

Institute of Biochemistry and Biotechnology

Martin Luther University Halle-Wittenberg

Kurt-Mothes-Str. 3a

06120 Halle (Saale)

Germany

ingo.heilmann@biochemtech.uni-halle.de

The class VIII myosin ATM2 stabilizes actin-plasma membrane contacts by locally promoting PtdIns(4,5)P_2 nanodomain formation in tobacco pollen tubes

Vera Wagner, Marta Fratini, Johanna Uhlenberg, Alexandra Schutkowski, Christoph Kastner, Kirsten Bacia, and Ingo Heilmann

Abstract

The intersection of actin-filaments with the plasma membrane in plant cells involves lipid-protein interactions by the Arabidopsis class VIII-myosin, ATM2 that are currently not understood. Using pollen tube cells as a model, we describe how ATM2 enables actin-plasma membrane contacts by modulating membrane lipid nano-organization. ATM2 binds both actin and phosphatidylinositol 4,5-bisphosphate (PtdIns(4,5)P_2), a lipid required for ATM2-plasma membrane-attachment. Overexpression of ATM2 unexpectedly stabilized actin-dynamics and altered pollen tube-morphology. Actin-dynamics remained unaltered upon overexpression of a lipid binding-defective ATM2-variant. ATM2-effects on actin-dynamics required PtdIns(4,5)P_2, as artificial PtdIns(4,5)P_2-depletion in pollen tubes abolished effects of full-length ATM2 on actin dynamics despite its retained plasma membrane-association. ATM2 colocalized and interacted with the PI4P 5-kinase, PIP5K2, which resides at actin-plasma membrane-contacts and forms PtdIns(4,5)P_2-nanodomains facilitating ROP-dependent actin-stabilization. Upon ATM2-overexpression, a fluorescent PtdIns(4,5)P_2-biosensor decorated an expanded plasma membrane-region *in vivo*, indicating a promoting effect of ATM2 on PtdIns(4,5)P_2-abundance. Moreover, catalytic activity of purified recombinant PIP5K2 protein was enhanced upon coincubation with a purified C-terminal ATM2-fragment *in vitro*, suggesting that ATM2 contributes to the intrinsic regulation of PtdIns(4,5)P_2-formation. Actin-dynamics are, thus, stabilized at the actin-plasma membrane interface by ATM2 locally promoting the formation of PtdIns(4,5)P_2-nanodomains, thereby self-reinforcing ATM2-recruitment while also facilitating ROP-activation to stabilize membrane-proximal actin-filaments.

Introduction

The extreme polarized morphology of pollen tubes or root hairs is a consequence of polar tip growth involving the focused transport of secretory vesicles towards a narrow plasma membrane area of the growing cell apex (Franciosini et al., 2016; Denninger et al., 2019; Guo and Yang, 2020; Orr et al., 2020; Fritz et al., 2024). The vectorial transport of vesicles, their fusion with the target membrane area, and the endocytic retrieval of vesicles upon cargo-release require the coordination of membrane trafficking and cytoskeletal dynamics in the cell apex (Samaj et al., 2006; Fu, 2015; Heilmann and Ischebeck, 2016; Grebnev et al., 2017; Guo and Yang, 2020; Fritz et al., 2024). Apart from their respective biological roles in plant sexual reproduction (Lord and Russell, 2002; Higashiyama and Takeuchi, 2015; Heilmann and Ischebeck, 2016) or in root/rhizosphere interactions (Muller and Schmidt, 2004; Denninger et al., 2019), pollen tubes or root hairs are ideal models to study the underlying molecular mechanisms of coordination, as cell morphology is critically altered by any perturbance in the coordination between membrane trafficking and cytoskeletal dynamics (Stenzel et al., 2008; Braga et al., 2023). In pollen tubes, the tip-directed trafficking machinery is focused towards a well-defined sub-apical plasma membrane domain enriched in the regulatory membrane lipid, phosphatidylinositol 4,5-bisphosphate (PtdIns(4,5)P_2) (Kost et al., 1999; Ischebeck et al., 2010a; Heilmann and Ischebeck, 2016). PtdIns(4,5)P_2 serves as a positional signal for the recruitment of proteins to the cytosolic face of the plasma membrane, and as such can exert different regulatory roles (Heilmann and Heilmann, 2025), including the regulation of secretion (Ischebeck et al., 2008; Sousa et al., 2008; Ischebeck et al., 2010b), endocytosis (Zhao et al.,

2010; Ischebeck et al., 2013), or the control of actin-dynamics (Ischebeck et al., 2011; Fratini et al., 2021). Pollen tube cells have been used extensively to study PtdIns(4,5)P_2-mediated coordination of membrane trafficking and cytoskeletal dynamics, as perturbations in the balance of these processes gives rise to characteristic changes in cell morphology, including pollen tube tip branching (Ischebeck et al., 2008; Ischebeck et al., 2010b) and related morphologies previously summarized as "secretion phenotypes" (Ischebeck et al., 2010b), or tip swelling associated with perturbed cytoskeletal stability (Ischebeck et al., 2011; Stenzel et al., 2012; Stenzel et al., 2020; Fratini et al., 2021). Moreover, pollen tubes are an ideal model to study the distribution of PtdIns(4,5)P_2, as the intrinsinc abundance of this lipid in pollen tubes is 20-30 times higher than in vegetative tissues (Fratini et al., 2021), thus enabling observations not currently possible in other plant cell types. Stabilized actin-dynamics upon PtdIns(4,5)P_2 overproduction has been shown in various biological systems, including mammalian cells (Fukami et al., 1992; Cremona and De Camilli, 2001), yeast (Desrivieres et al., 1998) and plants (Gungabissoon et al., 1998; Fratini et al., 2021), and while effects of PtdIns(4,5)P_2 on actin-dynamics are not limited to pollen tubes, the pollen tube model uniquely allows to investigate the molecular mechanisms of PtdIns(4,5)P_2-mediated regulation of actin-dynamics that are currently not understood in plants.

Several regulatory elements are known to be involved in the PtdIns(4,5)P_2-dependent control of actin-dynamics in plants, including monomeric rho of plants (ROP) GTPases (Kost, 2008; Yalovsky et al., 2008) and their effectors, such as guanine nucleotide dissociation inhibitors (GDIs) (Klahre et al., 2006; Yalovsky et al., 2008; Sun et al., 2015), which control the pool of ROPs that can be activated by plasma membrane-associated guanine nucleotide exchange factors (GEFs) (Klahre and Kost, 2006; Yalovsky et al., 2008), or ROP-interacting CRIB-domain containing (RIC) proteins (Wu et al., 2001; Hsu et al., 2010) representing key ROP targets. It has been proposed that PtdIns(4,5)P_2 controls the pool size of ROPs for GEF-mediated activation by serving as a GDI displacement factor (GDF) to facilitate the release of ROPs from GDI/ROP-complexes for activation (Kost, 2008; Ischebeck et al., 2011; Fratini et al., 2021). However, PtdIns(4,5)P_2 effects on pollen tube growth are not limited to the control of ROPs and actin-dynamics, and PtdIns(4,5)P_2 has additional, alternative roles in the control of secretion and endocytosis (Ischebeck et al., 2008; König et al., 2008; Ischebeck et al., 2013; Grebnev et al., 2017; Fritz et al., 2024). It is currently not well understood how alternative cellular processes appear to be specifically controlled by the little-abundant plasma membrane lipid, PtdIns(4,5)P_2.

One aspect guiding the coordination of alternative effects of PtdIns(4,5)P_2 on apical secretion or on cytoskeletal dynamics is a subcompartmentalized plasma membrane nanostructure, represented by clustered and non-clustered distribution of proteins and lipids, including PtdIns(4,5)P_2 (Fratini et al., 2021; Jaillais et al., 2024). Within the sub-apical plasma membrane zone of pollen tube cells, PtdIns(4,5)P_2 enriched in plasma membrane nanodomains has a focused stabilizing effect on actin-dynamics (Fratini et al., 2021). PtdIns(4,5)P_2 with a role in actin stabilization is formed by the nanodomain-associated PI4P 5-kinase, PIP5K2 (Stenzel et al., 2012; Fratini et al., 2021). It is currently unclear how PIP5K2 or PtdIns(4,5)P_2 interact with the actin cytoskeleton at the molecular level (Fratini et al., 2021) or what intrinsic molecular mechanisms control PtdIns(4,5)P_2 formation by PIP5K2. The plasma membrane-actin-interface is overall not well defined in plants, and plant genomes do not hold genes with similarity to those encoding proteins mediating actin-plasma membrane attachment in mammals or yeast (Yamamoto et al., 2001; Lacalle et al., 2007; Kawaguchi and Asano, 2022), such as the ERM protein family (Bretscher et al., 2002; Neisch and Fehon, 2011) or Nck proteins (Rivera et al., 2009). Despite the importance of actin-membrane attachment for plant physiology, there is currently only limited

information on how actin filaments intersect with the plasma membrane and what proteins or lipids mediate actin-plasma membrane contacts in plant cells.

Candidate proteins for mediators of actin-plasma membrane-attachment include myosins of the plant-specific myosin class VIII (Nebenfuhr and Dixit, 2018), which in Arabidopsis is represented by four isoforms, the proteins, ATM1 and VIIIA, and the pollen-specific ATM2 and VIIIB (Nebenfuhr and Dixit, 2018). Class VIII myosins display only minor motor activity compared to the better-characterized class XI myosins also found in plants (Nebenfuhr and Dixit, 2018). Myosins of classes VIII and XI have an overall similar domain architecture, with an N-terminal region containing an SRC-homology 3 (SH3)-domain, an actin-binding motor domain, a lever domain containing calmodulin-binding IQ motifs, a coiled-coil region likely mediating interactions between myosin monomers, and a C-terminal region mediating target/cargo interactions (Nebenfuhr and Dixit, 2018). Motor activity of myosins is thought to require the formation of myosin dimers (Haraguchi et al., 2014; Nebenfuhr and Dixit, 2018). However, not all myosins have been studied in this regard and while ATM1 binds with high affinity to actin (Haraguchi et al., 2014), it has been proposed that class VIII myosins might not require motor activity for their physiological function at all (Haraguchi et al., 2014; Nebenfuhr and Dixit, 2018). Phenotypic defects of Arabidopsis mutants with genetic lesions in genes for class VIII myosins suggest their involvement in a number of physiological processes. An Arabidopsis *atm1* mutant displays a decreased size of the root apical meristem and reduced cell proliferation in a sugar-dependent manner (Olatunji et al., 2023), and auxin signaling and transcriptional responses are dampened in roots of *atm1* mutants (Olatunji et al., 2023). Arabidopsis ATM2 has been implicated in endocytosis (Sattarzadeh et al., 2008). While the available data indicate a role of class VIII myosins in cytoskeletal control and/or endocytosis, the exact molecular function of class VIII myosins remains obscure. In tip-growing filament cells of the moss *Physcomitrium patens*, class VIII myosins mediate the interplay of actin and microtubules, thereby impacting on both cytoskeletal elements and ensuring that actin polymerization and cell expansion are localized properly in the expanding apex of the moss filaments (Wu and Bezanilla, 2014, 2018). These important studies establish a role of class VIII myosins in the spatio-temporal coordination of plant cytoskeletal structures. However, there is little information of how class VIII myosins might interact with membranes.

Based on the biochemical analysis of enriched recombinant myosin VIII fragments from Arabidopsis, we have previously reported that the pollen-expressed class VIII myosin, ATM2, binds anionic phospholipids and that a C-terminal polybasic region of ATM2 is necessary and sufficient for lipid binding and plasma membrane association of ATM2 in pollen tubes (Kastner et al., 2022). Importantly, ATM2 and other class VIII myosins display features consistent with a role in defining the actin-plasma membrane interface by binding both actin and anionic plasma membrane lipids through separate N-terminal and C-terminal domains, respectively (Haraguchi et al., 2014; Nebenfuhr and Dixit, 2018; Kastner et al., 2022). So far, it has not been demonstrated whether and how ATM2 mediates the attachment of actin to the plasma membrane and whether the action of ATM2 influences pollen tube expansion.

Here we show that association of ATM2 with the plasma membrane exerts a stabilizing effect on actin-dynamics in pollen tubes *in vivo*. ATM2 colocalizes and interacts with the PI4P 5-kinase, PIP5K2, in nanodomains and promotes PIP5K2-mediated PtdIns(4,5)P_2-formation *in vivo* and *in vitro*. Based on these observations, ATM2 may exert a dual effect by anchoring actin to plasma membrane PtdIns(4,5)P_2-nanodomains while at the same time stimulating PtdIns(4,5)P_2 formation, resulting in self-reinforcing promotion of PtdIns(4,5)P_2-dependent ATM2-recruitment and ROP-activation to mediate actin-stabilization at the actin-plasma membrane interface.

Results

The control of actin-plasma membrane contacts by regulatory lipids involves the class VIII myosin, ATM2 (Kastner et al., 2022). To our knowledge, plasma membrane association of ATM2 has not been analyzed at the nanodomain-scale, and possible physiological effects exerted by ATM2 on either actin or the plasma membrane have not been explored. Therefore, we aimed to characterize the distribution and function of ATM2, with a particular focus on its relations to the PI4P 5-kinase PIP5K2 and PtdIns(4,5)P_2, which together define plasma membrane nanodomains controlling actin-dynamics (Fratini et al., 2021).

ATM2 and PIP5K2 may define actin-plasma membrane contacts in a subapical PtdIns(4,5)P_2-enriched plasma membrane domain of pollen tubes.

In pollen tubes of various plant species, the extreme apical cytosol (the "clear zone") contains no larger organelles and is instead populated by secretory vesicles driving polarized cell expansion. The extent of the clear zone is defined by a fine network of dynamic peripheral actin filaments thought to guide vesicles to their respective sites of membrane insertion, or to remove endocytic vesicles (Fritz et al., 2024). The plasma membrane of the endocytotic zone of tobacco pollen tubes (Zonia and Munnik, 2008; Fritz et al., 2024) is occupied by membrane nanodomains decorated by a RedStar-PH_{PLC} marker (König et al., 2008) indicating the presence of PtdIns(4,5)P_2 (Fig. 1 A, left panels). A fluorescent marker for the class VIII myosin ATM2, EYFP-ATM2, occupies a very similar plasma membrane zone at the transition between the apical clear zone and the shank region of tobacco pollen tubes, where dynamic actin filaments are labeled by a coexpressed LifeAct-RFP marker (Riedl et al., 2008; Fratini et al., 2021) (Fig. 1 A, right panels). The PtdIns(4,5)P_2-biosensor and the EYFP-ATM2 marker, thus, occupy largely overlapping subapical plasma membrane regions in growing tobacco pollen tubes.

PtdIns(4,5)P_2 with a role in the control of actin-dynamics is formed by the PI4P 5-kinase, PIP5K2, which also resides in membrane nanodomains and causes pollen tube tip swelling due to its stabilizing effect on actin (Fratini et al., 2021). Plasma membrane nanodomains decorated by PIP5K2-EYFP intersected in pollen tubes with plasma membrane-oriented actin filaments labeled by the actin marker, LifeAct-RFP (Fig. 1 B). Computer-aided identification of regions of overlap of the fluorescent markers in subsets of confocal imaging stacks indicates plasma membrane nanodomains with a diameter < 1 µm as possible contact sites of actin filaments decorated by LifeAct-RFP with PIP5K2-EYFP at the plasma membrane (Fig. 1 B, lower panels). Please note that images shown in Fig. 1 B represent substacks and not individual confocal sections in order to capture the three-dimensional network of actin filaments. An EYFP-tagged N-terminal truncation of PIP5K2 located in a plasma membrane-proximal network-like pattern (Supplemental Fig. 1) differing from the distribution of EYFP-tagged full-length PIP5K2 (cf. Fig. 1 B), consistent with the previously reported role of the PIP5K2 linker (Lin)-domain in mediating plasma membrane nanodomain-association of the enzyme (Stenzel et al., 2012; Fratini et al., 2021) and indicating that PIP5K2 has a binding affinity to filamentous structures possibly representing membrane-peripheral actin (Supplemental Fig. 1). When mC-ATM2 was coexpressed with an mTalin-YFP marker for actin (Kost et al., 1998), we observed enhanced actin signals at the membrane-proximal ends of actin filaments intersecting with the plasma membrane (Fig. 1 C, arrowheads). The effects were observed upon expression of mC-fusions of Arabidopsis ATM2 (Fig. 1 C, left panels) as well as with fusions of tobacco ATM2 (NtMyo2-like; Fig. 1 , right panels), leading us to speculate on a possible stabilizing effect of ATM2 on actin at the plasma membrane-actin interface. Please note that images shown in Fig. 1 C represent

substacks and not individual confocal sections in order to capture the three-dimensional network of actin filaments. Based on the combined observations, we hypothesized that ATM2 and PIP5K2 might be part of a membrane-associated protein complex mediating and stabilizing actin-plasma membrane contacts.

Overexpression of ATM2 stabilizes actin-dynamics and induces tip swelling in pollen tube cells.

The observation of stabilized actin-plasma membrane contacts in pollen tube cells (Fig. 1 C) is consistent with previously observed apical swelling of tobacco pollen tubes overexpressing mC-ATM2 (Kastner et al., 2022), a cell morphology known to arise from a stabilized actin cytoskeleton, e.g., upon overexpression of ROPs (Klahre et al., 2006; Kost, 2008; Fritz et al., 2024) or PIP5K2 (but not PIP5K6) (Ischebeck et al., 2010b; Stenzel et al., 2012; Fratini et al., 2021). To determine whether or not the overexpression of ATM2 variants would mediate pollen tube tip swelling upon overexpression and whether this was related to a stabilized actin cytoskeleton, cell morphologies and actin-dynamics were assessed by laser scanning confocal microscopy in pollen tubes overexpressing mC-tagged variants of ATM2 (Fig. 2 A), including full-length ATM2 (mC-ATM2), a variant lacking the C-terminal lipid-binding domain (mC-ATM2$_{\Delta LB}$) or a C-terminal fragment of ATM2 lacking the actin-binding motor domain (mC-ATM2$_{CT}$), respectively, together with an actin marker, mTalin-YFP (Kost et al., 1998; Fratini et al., 2021) (Fig. 2 A). In control pollen tubes coexpressing an mC-protein and mTalin-YFP, actin was dynamic by kymograph analysis (Fig. 2 B, right panel) and occupied predominantly the shank region of the control cells (Fig. 2 B), in a pattern that was previously observed (Fratini et al., 2021). Moreover, the control cells displayed normal pollen tube cell morphology with tip diameters of approx. 10 µm (Fig. 2 B, D). By contrast, the expression of mC-ATM2 resulted in substantial pollen tube tip swelling (Fig. 2 B, D), in enhanced actin occupancy in the pollen tube tip region (Fig. 2 B, E), and in stabilization of actin-dynamics (Fig. 2 B, F). Quantitative analysis of pollen tube tip diameter (Fig. 2 D), tip actin occupancy (Fig. 2 E) and of mean actin lifetime (Fig. 2 F) indicate statistically significant effects. Deletion of the C-terminal lipid binding region of ATM2 in the mC-ATM2$_{\Delta LB}$ abolished plasma membrane association (Fig. 2 C) and the effect on actin-dynamics, and expression of mC-ATM2$_{\Delta LB}$ did not result in altered pollen tube tip width, altered actin occupancy, nor in altered actin-dynamics (Fig. 2 B, D-F). Similarly, the expression of mC-ATM2$_{CT}$ also had no effect on pollen tube tip width, on actin occupancy, nor on actin-dynamics, despite the retained plasma membrane association of this C-terminal ATM2-fragment (Fig. 2 B, D-F). Further quantitative analysis of the spatial persistence of actin signals indicates a significantly enhanced persistence of actin filaments upon expression of mC-ATM2, compared to the mC-controls or to tubes expressing mC-ATM2$_{\Delta LB}$ (Supplemental Fig. 2). The effect of mC-ATM2 on actin-dynamics is further characterized by terminal high-intensity signals of the mTalin-YFP marker on actin filaments (Fig. 2 B arrowheads; cf. Fig. 1 C). The data indicate an unexpected stabilizing effect of ATM2 on actin-dynamics, which requires membrane-association of full-length ATM2 via its C-terminal lipid binding region.

Artificial PtdIns(4,5)P_2 depletion at the plasma membrane abolishes ATM2 effects on actin-dynamics.

The deletion of the C-terminal lipid binding region of ATM2 abolished plasma membrane association and effects on actin-dynamics (Fig. 2 B-F). To verify the effect of the deletion, we assessed the influence of PtdIns(4,5)P_2 on the function of full-length ATM2 by modifying the pollen tube membrane lipid composition. The degree of actin stabilization by full-length ATM2 was monitored in pollen tube cells upon artificial depletion of PtdIns(4,5)P_2 by the coexpressed PtdIns(4,5)P_2-specific 5-phosphatase, PTase11 (Fig. 3). PTase11 specifically degrades PtdIns(4,5)P_2 to PtdIns4P and has previously been described as an enzyme that can counteract effects of increased PtdIns(4,5)P_2 biosynthesis in pollen tubes (Rausche et al., 2021). While coexpression with mC-PTase11 did not alter plasma membrane-

association of CFP-ATM2 (Fig. 3 B), the stabilizing effect of CFP-ATM2 on actin decorated by a mTalin-YFP marker in pollen tube cells was abolished (Fig. 3 A, B), resulting in morphologically normal cell shapes. In the presence of mC-Ptase11, CFP-ATM2 also no longer influenced tip actin occupancy or mean actin life time (Fig. 3 C, right panels). Similar data were obtained by using coexpression of full-length ATM2 with SAC9 (Williams et al., 2005; Lebecq et al., 2022), another PtdIns(4,5)P_2-specific 5-phosphatase of the suppressor of actin (SAC) family (Supplemental Fig. 3), indicating that the abolished function of ATM2 was a consequence of PtdIns(4,5)P_2 depletion, rather than an effect of any specific coexpressed enzyme.

To assess whether the artificial depletion of PtdIns(4,5)P_2 by mC-PTase11 specifically influenced the plasma membrane-proximal stabilization of actin by CFP-ATM2, we analyzed plasma membrane-proximal actin-dynamics by kymograph analysis for a mTalin-YFP marker, as indicated in Fig. 3 D (left panels). While the expression of CFP-ATM2 alone resulted in an enhanced lifetime of plasma membrane-proximal actin signals (Fig. 3 D), this effect was abolished to control levels upon coexpression of CFP-ATM2 with mC-PTase11 (Fig. 3 D), indicating that artificial depletion of PtdIns(4,5)P_2 rendered full-length ATM2 ineffective. While mC-ATM2 displayed pronounced plasma membrane association (cf. Fig. 2 B, C) that was lost upon deletion of the lipid-binding C-terminus in the mC-ATM2$_{\Delta LB}$ variant (cf. Fig. 2 B, C), interestingly the CFP-ATM2 marker retained plasma membrane association upon coexpression with mC-PTase11 (Fig. 3 A, B), even though effects of CFP-ATM2 on cell morphology or actin dynamics were abolished (Fig. 3 C, D). We conclude that lipid-mediated plasma membrane-recruitment of ATM2 is by itself not sufficient to enable its regulatory effects on actin, suggesting added regulatory interplay between ATM2 and PtdIns(4,5)P_2.

ATM2 displays a binding preference for PtdIns(4,5)P_2 *in vitro*.

To address a possible PtdIns(4,5)P_2-specific function of ATM2, we revisited lipid-binding characteristics of ATM2-derived protein fragments, ATM2$_{CT}$, or ATM2$_{CT\Delta LB}$ additionally lacking the C-terminal 43 residues representing the polybasic lipid-binding region (Fig. 4). In previous analyses, a recombinant C-terminal fragment of ATM2 bound to various anionic plasma membrane lipids *in vitro*, with no clear preference for any particular lipid (Kastner et al., 2022). Here, purified recombinant ATM2$_{CT}$ carrying a C-terminal His$_6$-tag (ATM2$_{CT}$-His$_6$) again bound to various lipids in *in vitro* lipid overlay assays (Fig. 4 A), including to all phosphoinositides with the exception of PtdIns5P, and to phosphatidic acid. By contrast, the ATM2$_{CT\Delta LB}$-His$_6$ variant displayed no detectable binding to any lipids, similar to the negative control, His$_6$ (Fig. 4 A, as indicated). A drawback of the lipid overlay assay is that lipids are presented in very high abundance but not in a membraneous formulation, and it may be difficult to assess quantitative differences in lipid binding by this method (Heilmann and Heilmann, 2025). Therefore, we analyzed lipid binding of enriched recombinant fusions of ATM2-fragments to superfolder GFP (sfGFP) (Fig. 4 B) by using microscale thermophoresis (MST) for a more quantitative biochemical approach (Fig. 4 C-F). MST can be used to assess protein-lipid interactions (Sparks and Fratti, 2019). Importantly, for MST lipid ligands can be presented in the form of liposomes, representing a lipid regime that more closely resembles a biological membrane (Julkowska et al., 2013). Here, we used dioleoyl-phosphatidylcholine (DOPC) as a liposome backbone, to which 20 mol% of either PtdIns(4,5)P_2 or of PtdIns4P were added (Fig. 4 C). These lipids were chosen for analysis, because they are the substrate and product, respectively, of AtPTase11, which exerted a relevant effect on ATM2 function *in vivo* (cf. Fig. 3). The MST analysis shows that a super-folder GFP (sfGFP)-tagged C-terminal fragment of ATM2 bound to PtdIns(4,5)P_2 with a 3-fold higher affinity than to PtdIns4P (Fig. 4 C, F). There was no detectable binding of the sfGFP-tag alone to either liposome regime used (Fig. 4 D). To further support the imaging data on the C-terminal truncation of ATM2 (cf. Fig.

2), we applied the MST measurement also to compare PtdIns(4,5)P_2 binding by sfGFP-ATM2$_{CT}$ vs. the truncated sfGFP-ATM2$_{CT\Delta LB}$ variant. Deleting the C-terminal lipid binding region of ATM2 resulted in a 99.5 % reduction of PtdIns(4,5)P_2-binding affinity (Fig. 4 E, F). The data confirm that the C-terminal portion of ATM2 is necessary and sufficient for the ATM2-lipid interaction.

ATM2 promotes PtdIns(4,5)P_2 formation by PIP5K2 *in vivo* and *in vitro*.

While the preference of ATM2 for binding to PtdIns(4,5)P_2 is consistent with the effects of PIP5K2 (Fratini et al., 2021) or PTase11 on ATM2 function in controlling actin-dynamics (cf. Fig. 3), we next asked whether a 3-fold difference in binding affinities to PtdIns(4,5)P_2 vs. PtdIns4P might provide a sufficient molecular basis for the PtdIns(4,5)P_2-dependency of the regulating effect of ATM2 on actin. Both the deletion of the lipid binding domain in ATM2 and the depletion of plasma membrane PtdIns(4,5)P_2 by PTase11 abolished ATM2 effects on actin-dynamics, leading us to speculate that an additional, plasma membrane-associated process exerts a relevant contribution to actin stabilization by ATM2. When analyzed by spinning disc microscopy, the localization of an EYFP-ATM2 marker substantially coincided with the distribution of a RedStar-PH$_{PLC}$ biosensor for PtdIns(4,5)P_2 at the plasma membrane of tobacco pollen tubes (Fig. 5 A), consistent with the preferred *in vitro* binding of ATM2 to PtdIns(4,5)P_2 (cf. Fig. 4). While analyzing the distribution of the RedStar-PH$_{PLC}$ biosensor upon coexpression of different ATM2 variants, we observed that the distribution of the RedStar-PH$_{PLC}$ marker was influenced by coexpression with the plasma membrane-associating EYFP-ATM2, but not by coexpression with the lipid-binding-deficient variant, EYFP-ATM2$_{\Delta LB}$ (Fig. 5 B): The extent of the subapical plasma membrane domain marked by RedStar-PH$_{PLC}$ was substantially enhanced when EYFP-ATM2 was expressed, whereas a much smaller effect was observed upon expression of EYFP-ATM2$_{\Delta LB}$ (Fig. 5 B). Importantly, the area density of plasma membrane nanodomains decorated by RedStar-PH$_{PLC}$ (Fratini et al., 2021) was not significantly altered in the expanded plasma membrane regions (Fig. 5 B, bottom right), indicating a promoting effect of plasma membrane-associated EYFP-ATM2 on PtdIns(4,5)P_2 production. As PtdIns(4,5)P_2 with a role in controlling actin-dynamics is formed in plasma membrane nanodomains by PIP5K2 (Fratini et al., 2021), we next used split-ubiquitin-based yeast two hybrid analysis to test for interactions between PIP5K2 and different myosins representing the two plant-specific myosin classes VIII or XI (Fig. 5 C, left panels). The data suggest interactions of PIP5K2 with both class VIII myosins tested but with none of the class XI myosins (Fig. 5 C, left panels). Moreover, the functionally divergent PI4P 5-kinase isoform, PIP5K6, which does not localize in plasma membrane nanodomains and does not influence actin-dynamics when expressed in pollen tubes (Fratini et al., 2021), displayed no interaction with any of the myosins tested in the split-ubiquitin-based yeast-two-hybrid analysis (Fig. 5 C, right panels). To test whether a possible interaction of ATM2 with PIP5K2 exerted an effect on PtdIns(4,5)P_2 formation, we next performed *in vitro* PI4P 5-kinase activity tests with purified recombinant PIP5K2 protein in the absence or presence of purified recombinant fragments of ATM2 or VIIIB proteins (Fig. 5 D, E). All proteins were recombinantly expressed in *E. coli*, PIP5K2 as a fusion to an N-terminal maltose-binding protein (MBP)-tag and a C-terminal His_6-tag (Ischebeck et al., 2013), and C-terminal fragments of ATM2 or VIIIB as fusions to N-terminal His_6-tags (Kastner et al., 2022). The *in vitro* lipid phosphorylation assays with PtdIns4P substrate (Fig. 5 D) show that PtdIns(4,5)P_2 formation by MBP-PIP5K2 (closed arrowhead) was substantially enhanced by the addition of either class VIII myosin-fragment, His_6-ATM2 or His_6-VIIIB (Fig. 5 D, E). A negative control using *E. coli* extract alone did not result in PtdIns(4,5)P_2 formation (Fig. 5 D). Further PIP5K2 activity assays were performed in the presence of recombinant wild type ROP2 from Arabidopsis or its constitutive active or dominant negative substitution variants, ROP2 G15V or ROP2 T20N (Feiguelman et al., 2018), respectively, and these proteins all had no effect on PtdIns(4,5)P_2 formation by PIP5K2 (Fig. 5 E). The *in*

vitro activity tests with purified recombinant proteins are consistent with a direct physical interaction between ATM2 and PIP5K2 exerting a regulatory effect. Importantly, the enhanced *in vitro* activity of PIP5K2 in the presence of ATM2 or VIIIB fragments indicates that PtdIns(4,5)P_2 formation is promoted by the presence of the myosin fragments, with no requirement for further elements. In sum, the data from the *in vivo* observation of altered distribution of the PtdIns(4,5)P_2 biosensor, RedStar-PH_{PLC}, in tobacco pollen tubes (Fig. 5 B) and from *in vitro* experiments (Fig. 5 D, E) are consistent with a promoting effect of ATM2 on the formation of PtdIns(4,5)P_2 in the plasma membrane of pollen tube cells.

ATM2 acts in a common pathway with elements of ROP signaling

The functional interplay of ATM2 with PtdIns(4,5)P_2 and PIP5K2 (cf. Figs. 3-5) suggested that ATM2 might act in the same physiological context as PIP5K2, which has previously been shown to influence ROP-dependent cytoskeletal control (Fratini et al., 2021). Specifically, PtdIns(4,5)P_2 formed by PIP5K2 has been proposed to act as a GDF, mediating the release of ROP proteins from GDI-ROP complexes for activation (Kost, 2008; Ischebeck et al., 2011; Fratini et al., 2021). As ATM2 activated PIP5K2 and promoted PtdIns(4,5)P_2 formation, we next investigated a possible functional interplay between ATM2 and the GDI protein, NtRhoGDI2 (Klahre et al., 2006; Fratini et al., 2021) (Fig. 6). Initial yeast-two-hybrid analyses indicated interaction of NtRhoGDI2 with PIP5K2 (Fig. 6 A, left panel) as well as with ATM2 (Fig. 6 A, right panel). A functional interaction of ATM2 with NtRhoGDI2 is further supported by the observation that coexpression of NtRhoGDI2-EYFP influenced the plasma membrane distribution of mC-ATM2. An mC-ATM2 marker expressed in tobacco pollen tubes distributed over a much smaller, more apical plasma membrane region when coexpressed with NtRhoGDI2-EYFP, compared to a more relaxed plasma membrane distribution upon coexpression with an EYFP-control (Fig. 6 B). Quantitative analysis of the respective distribution patterns indicates that the difference was significant (Fig. 6 C, D), and most pronounced in the transition zone between clear zone and the shank region of the pollen tube (Fig. 6 E, cf. Fig. 1 A). As furthermore the coexpression of mC-ATM2 with NtRhoGDI2-EYFP also resulted in significantly reduced pollen tube tip swelling compared to that upon coexpression of mC-ATM2 with an EYFP control (Fig. 6 F), we conclude that ATM2 acts in a common pathway with PIP5K2/PtdIns(4,5)P_2, ROPs and NtRhoGDI2.

Discussion

ATM2 stabilizes actin-dynamics at the plasma membrane-actin interface through lipid-binding and protein-protein interactions

ATM2 is thought to contribute to forming an actin-plasma membrane interface by binding to actin via its N-terminal actin-binding region, and to the plasma membrane via its C-terminal polybasic lipid-binding domain (Kastner et al., 2022). Here we show that ATM2 is not only a tether for actin filaments at the plasma membrane, but that ATM2 exerts an active stabilizing effect on actin-dynamics (Fig. 1 C, Fig. 2). The stabilizing effect of ATM2 on actin-dynamics in pollen tubes resembles that of overproducing ROPs (Klahre and Kost, 2006), or PtdIns(4,5)P_2 via overexpressing nanodomain-associated PIP5K2 (Stenzel et al., 2012; Fratini et al., 2021). Our data provide information on the so-far-elusive molecular role of class VIII myosins, which serve as adaptors between actin filaments and the plasma membrane and exert a stabilizing effect on actin that is linked to the molecular function of ROPs (Kost et al., 1999; Klahre et al., 2006; Klahre and Kost, 2006; Kost, 2008; Fritz et al., 2024) and PtdIns(4,5)P_2 (Ischebeck et al., 2011; Stenzel et al., 2012; Fratini et al., 2021).

Clearly, binding to PtdIns(4,5)P_2 is required for ATM2-mediated effects on actin-dynamics, based on the two key findings, (i) that overexpression of the lipid-binding-deficient ATM2$_{\Delta LB}$ truncation did not exert an effect on actin-dynamics in tobacco pollen tubes (Fig. 2 B-F); and (ii) that effects of full-length ATM2 on actin-dynamics were abolished upon coexpression with the PtdIns(4,5)P_2-degrading enzymes, PTase11 (Fig. 3) or SAC9 (Supplemental Fig. 3). As the expression of the PtdIns(4,5)P_2-binding portion of ATM2, mC-ATM2$_{CT}$, did not influence actin-dynamics or cell morphology in pollen tubes (Fig. 2 B, D-F), we conclude that the N-terminal half of ATM2 also has a role in mediating ATM2-effect on actin-dynamics, possibly by mediating interactions with actin, or with other relevant proteins. As actin stabilization by ATM2 was observed mostly at the plasma membrane (arrowheads in Figs. 1 C, 2 B; and Fig. 3 D), we furthermore conclude that a plasma membrane-proximal process mediates ATM2-effects on actin-dynamics. Interestingly, plasma membrane-association of CFP-ATM2 was retained in the presence of mC-PTase11 (Fig. 3 A, B) or of SAC9 (data not shown), which upon coexpression nonetheless both suppressed ATM2-mediated effects on actin-dynamics and cell morphology (Fig. 3 A, C). As PTase11 and SAC9 convert PtdIns(4,5)P_2 to PtdIns4P, which might still mediate membrane-association of ATM2, we conclude that the PtdIns(4,5)P_2-dependent actin-stabilizing effect of ATM2 involves not only membrane recruitment of ATM2, and that the observed activation of PIP5K2 and enhanced PtdIns(4,5)P_2-formation (Fig. 5) were relevant in this context.

ATM2 activates PIP5K2, promoting PtdIns(4,5)P_2 nanodomains

So far, for plant models it has remained elusive what intrinsic molecular mechanisms control how and when PtdIns(4,5)P_2 is formed. Previous reports on the effects of PtdIns(4,5)P_2 have relied on the artificial perturbation of PtdIns(4,5)P_2 formation, e.g., by artificially overproducing or underproducing PtdIns(4,5)P_2 (Ischebeck et al., 2008; Sousa et al., 2008; Ischebeck et al., 2010b; Zhao et al., 2010; Ischebeck et al., 2011; Stenzel et al., 2012; Ischebeck et al., 2013; Stenzel et al., 2020; Fratini et al., 2021), demonstrating an essential involvement of PtdIns(4,5)P_2 in secretion (Ischebeck et al., 2008; Ischebeck et al., 2010b), endocytosis (Zhao et al., 2010), or in the control of actin-dynamics (Ischebeck et al., 2011; Fratini et al., 2021). However, only few studies inform on how PtdIns(4,5)P_2 formation might be intrinsically regulated. For instance, the Arabidopsis PI4P 5-kinase PIP5K6 can be regulated by phosphorylation (Hempel et al., 2017), and this regulation might be relevant for plant responses to pathogen infection (Menzel et al., 2019). Phosphorylation of plant PI4P 5-kinases has also been reported for barley, but so far with unclear effect (Saake et al., 2025). There is currently no report of intrinsic regulation of PIP5K2 with a role in controlling actin-dynamics.

The observation of altered fluorescence distribution of the PtdIns(4,5)P_2-biosensor, RedStar-PH$_{PLC}$ upon coexpression with ATM2-EYFP (Fig. 5 B) indicates that ATM2 might contribute to the intrinsic regulation of PtdIns(4,5)P_2-production *in vivo*. In pollen tubes, PtdIns(4,5)P_2 with a role in controlling actin-dynamics is mainly formed by the enzyme, PIP5K2 (Stenzel et al., 2012; Fratini et al., 2021). Yeast-two-hybrid analysis (Fig. 5 C) and the direct *in vitro* activation of purified recombinant PIP5K2 protein by a purified recombinant C-terminal ATM2 fragment (Fig. 5 D, E) indicate that an interaction between ATM2 and PIP5K2 might modulate PtdIns(4,5)P_2 formation by PIP5K2. Our data are consistent with an intrinsic regulatory effect of ATM2 on PtdIns(4,5)P_2 formation by PIP5K2, which *in vivo* will likely be occurring in plasma membrane nanodomains occupied by PIP5K2 (Fratini et al., 2021).

In the absence of structural information on the proposed PIP5K2/ATM2 complex, it remains unclear how the ATM2-mediated activation of PIP5K2 can be rationalized at the protein-structural level. Based on the *in vitro* data, it appears that the interaction between the C-terminal portion of ATM2 with PIP5K2 is

sufficient to promote enhanced PtdIns(4,5)P_2 formation (Fig. 5 D, E). It has previously been proposed that the plant-specific N-terminal domains of Arabidopsis PIP5K1 exerts an autoinhibitory role (Im et al., 2007). As PIP5K1 is 87 % identical in sequence to PIP5K2, it is possible that PIP5K2 is also autoinhibited by self-interaction between the catalytic domain of the enzyme with its N-terminal regulatory domains, as previously postulated for PIP5K1 (Im et al., 2007). The linker (Lin)-region between the catalytic domain and the N-terminal domains of PIP5K2 is of key importance for the association of PIP5K2 with plasma membrane nanodomains (Fratini et al., 2021), and also specifically for the effect of PIP5K2 on actin-dynamics (Fratini et al., 2021), leading us to speculate that the Lin-region might mediate protein-protein interactions with proteins in plasma membrane nanodomains mediating actin-plasma membrane contacts. As ATM2 is an interacting protein acting in this context, it appears plausible that an interaction of ATM2 with the Lin-region of PIP5K2 might interfere with the proposed autoinhibition, thereby effecting an activation of PIP5K2 and enhanced PtdIns(4,5)P_2 production. While this scenario is consistent with previously published data on the catalytic behavior of plant PI4P 5-kinases (Im et al., 2007; Stenzel et al., 2012), in the absence of structural information the exact molecular mechanism of ATM2-mediated activation of PIP5K2 remains currently unresolved. Current research is directed towards using combined molecular modeling and experimental protein structure determination approaches to determine the details of PIP5K2 activation by ATM2 at the structural level.

A self-reinforcing regulatory loop to stabilize actin-plasma membrane attachment

ATM2 effects on actin tie into the system of known regulators of actin-dynamics, and the requirement for lipid-binding places ATM2 downstream of PtdIns(4,5)P_2 production (cf. Figs. 2-4). However, the regulation of actin-dynamics is not a linear series of events, as illustrated in the model schematic in Fig. 7. While ATM2 binds to PtdIns(4,5)P_2 via its C-terminal polybasic region (Fig. 5 C, D), and this binding is required for downstream ATM2 effects on actin-dynamics (Fig. 2), ATM2 also acts upstream of PtdIns(4,5)P_2 by promoting PtdIns(4,5)P_2-production at the plasma membrane (Fig. 5). The ensuing mutual interdependencies between ATM2, PIP5K2-activation and PtdIns(4,5)P_2-formation illustrated in Fig. 7 introduce an element of self-reinforcement that might explain why ATM2 effects on actin-dynamics may require plasma membrane association. By interacting at the plasma membrane with PIP5K2, ATM2 will promote the production of PtdIns(4,5)P_2, attracting more ATM2, releasing more ROP for activation at the plasma membrane (Kost, 2008), and thus promote actin stabilization (Fig. 7). The interaction between ATM2 and PIP5K2, thus, might locally - and likely also transiently - potentiate PtdIns(4,5)P_2 production to mediate efficient recruitment stabilization of actin. In this scenario, only PtdIns(4,5)P_2-production is locally promoted, making the process PtdIns(4,5)P_2-dependent without a requirement for high-affinity preferential binding of ATM2 to any specific lipid. The proposed self-reinforcing loop between PtdIns(4,5)P_2-dependent recruitment of ATM2 and ATM2-dependent promotion of PtdIns(4,5)P_2 formation by PIP5K2 might, thus, contribute to the intrinsic regulation of PIP5K2 and PtdIns(4,5)P_2 abundance at actin-plasma membrane contact sites.

Methods and Protocols

Plant materials and growth conditions

Wild-type *Nicotiana tabacum* (ecotype Samsun N) plants were grown on soil in a greenhouse at 21°C–26°C and ambient humidity under long-day conditions (16 h light, 8 h darkness) and semi-controlled light intensities. The pollen was harvested from mature flowers after 8-9 weeks of cultivation and directly used.

cDNA constructs

Constructs for transient expression in pollen tubes. The actin marker constructs LifeAct-RFP and mTalin-YFP were described previously (Fratini et al., 2021). The RedStar-PLC_{PH} construct was assembled as previously described (Ischebeck et al., 2010b). The *ATM2* coding sequence was amplified from Arabidopsis flower cDNA using the primer combination 5’- ATGCGGCGCGCCATGATGTTATCGGCATCG-3’/5’-ATGCCTCGAGCTAGCCTCTTTTTCCCCACC-3’. The coding sequence for $ATM2_{\Delta LB}$ ($ATM2_{1\text{-}1177}$) was amplified using the primers 5’-ATGCGGCGCGCCATGATGTTATCGGCATCG-3’/5’-ATGCGCGGCCGCCTAAAATTCATCTTCTGG-3’. For *$ATM2_{CT}$* ($ATM2_{972\text{-}1220}$), the primers 5’-ATGCGGCGCGCCATGCGCAATGTGGCGACA-3’ and 5’-ATGCCTCGAGCTAGCCTCTTTTTCCCCACC-3’ sites were used. The coding sequence for tobacco NtMyo2-like isoform X2 was amplified from tobacco (*N. tabacum*) cDNA, using the primer combination 5'- ATGCGGCGCGCCATGTTGTCCGTTTCGCATAA-3'/5'-ATGCGCGGCCGCTCACTTGCTCTTCTTACCCCA-3'. Amplicons were moved as AscI/XhoI or AscI/NotI fragments into pEntry:pLAT52 vectors in frame with the coding sequences for EYFP, mCherry, or CFP. The constructs mC-AtSAC9 or mC-AtPTase11 were identical to those previously reported (Rausche et al., 2021). For AtPTase11, the coding sequence was additionally excised with XhoI and NotI and cloned downstream of the pEntry:pLAT52:mCherry cassette.

Constructs for recombinant expression. The construct encoding ATM_{CT}-His_6 (representing $ATM2_{972\text{-}1220}$-His_6) for bacterial expression was used as described previously (Kastner et al., 2022). The *$ATM2_{CT\Delta LB}$-His_6* construct (representing $ATM2_{972\text{-}1177}$-His_6) was generated using the primer combination 5’-ATCGCATATGCGCAATGTGGCGACAAAA-3’/5’-ATCGGGATCCCTAAAATTCATCTTCTGG-3’ restriction sites and moved into pMalc5G as an NdeI/BamHI fragment. Cloning of the His_6-MBP-construct (Stenzel et al., 2008) and the *MBP-PIP5K2* construct (Hempel et al., 2017) were described previously. To optimize protein enrichment and detection, a C-terminal His_6-tag was added by site directed mutagenesis using the primers 5'-ACCACCACCACTAGAGTCGACGGAT-3'/5'-CCGGTGGTGAGCGTCTTCAA-3'. For sfGFP fusion constructs, the *sfGFP* coding sequence was amplified using the primers 5’-ATGCCCATGGAAAGTAAAGGCGAAGAGCTGTT-3’ and 5’-ATGCGGATGGACGAGCTGTATAAACATATG-3’ and moved as an NcoI/NdeI-fragment into *pET28b*. the *$ATM2_{CT}$* coding sequence was amplified using the primers 5’-ATCGGTCGACATGCGTAATGTTG-3’/5’-ATCGGGCAAACGTGGCGCGGCCGC-3’ and moved in frame downstream of sfGFP as a SalI/ NotI-fragment. The coding sequence for the truncated variant $ATM2_{CT\Delta LB}$ was amplified using the primers 5’-ATCGGTCGACATGCGTAATGTTG-3’/5’-ATCGCAGAAGATGAATTTGCGGCCGCA-3’, and the amplicon was moved into *pET28b* in frame behind sfGFP as a SalI/NotI fragment, generating a C-terminal His_6 fusion.

Constructs for yeast-two-hybrid analysis. The pBT3-C-OST4 constructs for using PIP5K2 or PIP5K6 as baits were used as described previously (PIP5K2 (Gerth et al., 2017) or PIP5K6 (Hempel et al., 2017)). The coding sequences for the respective C-terminal myosin-fragments used as prey proteins were amplified using the following primer combinations: $ATM2_{972\text{-}1220}$, 5'-ATGCGGCCATTACGGCCCGCAATGTGGCGACAAAATCAAAG-3'/5'-ATGCGGCCGAGGCGGCCCTAGCCTCTTTTTCCCCACC -3'; $VIIIB_{921\text{-}1134}$, 5'-ATGCGGCCATTACGGCCCGCAATGAGAAGAAAAAAAC-3'/5'-ATGCGGCCGAGGCGGCCTCAATAACTTTTCTTGCACC-3'; $XI\text{-}1_{881\text{-}1520}$, 5'-ATGCGGCCATTACGGCCACCGGTGCTCTTAAAGATGC-3'/5'-ATGCGGCCGAGGCGGCCTCAATCTGACCTTTCCAACAAG-3'; $XI\text{-}2_{883\text{-}1505}$, 5'-ATGCGGCCATTACGGCCACTGGAGCACTCCAAGCAGCC-3'/5'-

ATGCGGCCGAGGCGGCCTTAGTGCAAGAATACAAATG-3'; XI-$A_{883-1730}$, 5'-
ATGCGGCCATTACGGCCACAGGAGCACTTCAAGATGC-3'/5'-
ATGCGGCCGAGGCGGCCTCATTCCTTGAGAAAGAGGAAG-3'; XI-$C_{892-1538}$, 5'-
ATGCGGCCATTACGGCCACAGGAGCACTTAAAGAGGC-3'/5'-
ATGCGGCCGAGGCGGCCTCACTCAGAGACTGGCAATAAG-3'; XI-$E_{887-1529}$, 5'-
ATGCGGCCATTACGGCCACAGGCGCACTGAAAGAGGC-3'/5'-
ATGCGGCCGAGGCGGCCTTAGTCAGAACATGGCAATAG-3'; XI-$H_{890-1516}$, 5'-
ATGCGGCCATTACGGCCACGGGAGTCCTTGAAGCTGCC-3'/5'-
ATGCGGCCGAGGCGGCCTTATATCAAGAAACTGAAAGC-3'; XI-$I_{889-1522}$, 5'-
ATGCGGCCATTACGGCCCTTGAGAAACGATTGAGAAC-3'/5'-
ATGCGGCCGAGGCGGCCTCAAATGATCTGCTTTGAGG-3'. Amplicons were moved as SfiI/SfiI-fragments into pPR3-N.

Expression and enrichment of recombinant proteins in *E. coli*

Recombinant proteins were generated as previously described (Stenzel et al., 2012; Hempel et al., 2017; Kastner et al., 2022). In brief, ATM2 variants were expressed in *E. coli* Rosetta 2 (DE3) cells (genotype F– ompT hsdSB(rB– mB–) gal dcm (DE3) pRARE2 (CamR) (Merck, Darmstadt, Germany). Precultures were grown over night in 50 ml liquid 2 YT media 1% (w/v) yeast extract, 1.6% (w/v) tryptone, 0.5% (w/v) NaCl, 0.2% (w/v) glucose) at 37 °C shaking at 150 rpm and used to inoculate 1 l (ATM2) or 3 l (PIP5K2) 2 YT cultures at 0.1 optical density (600 nm) units. Expression cultures were grown in 5 l baffled flasks at 37 °C shaking at 120 rpm to an optical density (600 nm) of 0.8 units. Expression of recombinant proteins was induced by adding 0.1 mM isopropyl β-d-thiogalactopyranoside and incubating for 4 h (ATM2) or for 2 h (PIP5K2) at 22 °C. Enrichment of recombinant proteins or protein fragments was performed as previously described; MBP-PIP5K2 (Dejonghe et al., 2016); C-terminal fragments of VIII-B or ATM2 (Kastner et al., 2022). His_6-tagged sfGFP fusions were enriched by Ni^{2+}-affinity chromatography using 5 ml HisTrap HP (Sigma-Aldrich, Munich, Germany) columns and an ÄKTA FPLC (GE Healthcare, München, Deutschland) according to manufacturer's instructions.

Transient expression of cDNA constructs in tobacco pollen tubes

Transient expression of cDNA constructs in tobacco pollen tubes was achieved by particle bombardment exactly as previously described (Fratini et al., 2021).

Confocal microscopy

Images were acquired using a Zeiss LSM880 Airyscan system or a Zeiss Cell observer with a Yokogawa CSU-X1 spinning disc (SD) unit. For LSM880 imaging, a 40× objective without immersion was used, and images were captured with the ZEN Black image analysis software with the pinhole set to 1 Airy Unit. Distribution and dynamics of actin filaments were obtained by using mTalin-YFP as an actin marker. YFP emission was detected at 514 nm using a HFT 514-nm main beam splitter. Z stacks of 2 µm slices were captured as time-lapses of 10 s intervals over the course of 5 min (30 cycles) using the high-resolution z piezo.

For localisation studies, z stacks and time series were captured by SD microscopy. Images were acquired using 63x oil immersion. Firstly, the cytoplasmic streaming was checked by brightfield acquisition as time-lapse with 10s/18 cycles (3 min). Z stacks were acquired in 0.3 µm slices. The acquisition time for constructs fused to EYFP was 400-600 ms; for mCherry/RFP 700-900 ms at 25% laser power.

Image Analysis

Pollen tubes tip-width was determined by measuring the diameter in the apical region either on brightfield images or fluorescence snapshots using the Fiji software package (Schindelin et al., 2012).

Actin-dynamics were analysed as previously described (Fratini et al., 2021; Braga et al., 2023). In brief, Z image stacks were analyzed over a 5-min time series with excitation of the YFP of the actin marker mTalin-YFP. Stacks were converted to Z projections with maximum intensity using Fiji (Schindelin et al., 2012). Backgrounds were subtracted using a rolling ball radius of 30 pixels. Due to the strong difference in fluorescence intensities between the pollen tube tip and the basal region of the tube, projections were divided into tip and body and analysed separately. Kymographs were generated from the tip region and analysed without bias for the length of the fluorescence signals using the machine learning program Ilastik via segmentation and pixel classification (Berg et al., 2019). The euclidean diameter of the segments was extracted, and segments <5 pixels were excluded as background. Further quantitative analysis of the actin-dynamics was carried out using Excel. The lengths of the fluorescence signals of the kymographs of all evaluated pollen tubes were normalised against the width of the total length of the kymograph (in pixels). As a measure for actin-dynamics, the mean lifetime of the actin signals was then calculated using the normalised values.

Actin occupany was analyzed by extracting the median plane of the z projections for actin dynamic analysis, and pixel size of both actin filaments and pollen tube tip was assessed using ilastik. The ratio of both values was used for calculating the occupancy in %. To analyze plasma membrane–actin attachment, the plasma membrane was marked in Z-projections with a segmented line, kymographs were generated using the reslice function in Fiji, and mean lifetimes were calculated.

To examine the spatial correlation between ATM2 and RedStar-PH_{PLC}, the first (most peripheral) optical section of the Z-stacks recorded by SD was analyzed. Fluorescence channels were examined individually. Global colocalization was quantified using the Manders coefficient function implemented in the Fiji plugin JACoP (Bolte and Cordelieres, 2006). For local colocalization, manually selected ATM2 domains were saved as regions of interest (ROIs) and analyzed separately.

To visualize overlap between ATM2 and RedStar-PH_{PLC}, surface sections acquired by SD were split into individual channels and converted into binary images by thresholding. The overlapping regions were identified using the image calculator, saved as ROIs, and then overlaid onto the original image for visualization.

For quantifying the area density of RedStar-PH_{PLC} signals at the pollen tube tip, the first slice of SD acquired z projections was extracted. Pixel sizes were determined using ilastik and presented as a ratio to the membrane area analyzed. To further quantify the distribution of the signals, the z projection was used to extract exact x and y coordinates using the Fiji plugin TrackMate (Tinevez et al., 2017).

Fluorescence intensity profiles were obtained from SD images. Using ImageJ, a segmented line was manually drawn along one side of the plasma membrane from the tip toward the shank. The selection was straightened (width 10 pixel) to generate a tip-to-shank membrane projection. Extracted fluorescence intensity profiles were normalized to a 0-1 intensity range. For the visualisation of the spatial distribution of the mC-ATM2 signal, normalized intensity values ±SEM were plotted. To obtain the dimension of mC-ATM2 domains, the spatial expanse of the signal was determined as a continuous membrane segment with normalized intensity ≥0.3. To distinguish between tip-focused or shank

distribution, normalized intensities were calculated for the apical tip region (0-20 µm) and the adjacent shank region (20-40 µm) for each profile.

Statistical Evaluation

Statistical evaluation was performed as indicated, using ANOVA with post hoc Tukeys test performed using R; or for pairwise comparisons by two sample t-test, assuming pooled-variance with unknown equal standard deviation, performed using statskingdom.de.

***In vitro* lipid phosphorylation assay**

The catalytic activity of recombinant PI4P5-kinases was determined by their ability to phosphorylate PtdIns4P in the presence of [γ-^{32}P]ATP, following established procedures (Heilmann et al., 2001). In brief the lipid substrate PtdIns4P (Avanti) was sonicated in the presence of Triton X-100 for 10 min in a sonicating bath. Afterwards recombinant lipid kinase was mixed with or without ATM2 and 10 µCi [γ-^{32}P]ATP was added. The reaction was started by combining lipid and protein components. The reaction mix was incubated at room temperature for 15 min. Lipids were extracted using acidic phase-separation. Radiolabeled lipid reaction products were separated by thin layer chromatography and visualized by autoradiography. Incorporation of ^{32}P was quantified by phosphorimaging using an Amersham Typhoon scanner (GE), BAS imaging screens (Fujifilm) and Image Quant software.

Protein lipid overlay assay

Protein–lipid overlay assays were performed using commercial "PIP strips" (Echelon Biosciences) containing 100 pmol of each immobilized lipid, as indicated. Strips were blocked with 3% (w/v) milk powder in TBS buffer, washed three times with TBS, and incubated for 45 min to 1 h with 0.5–2.5 mg ml^{-1} protein in 3% (w/v) BSA with gentle shaking. After three additional washes with TBS, strips were incubated with primary antibody (mouse anti-penta-His, BSA-free, Qiagen, Hilden, Germany, cat. no. 34670, diluted at 1:2000) for 1 h at room temperature or overnight at 4 °C. After two washes with TBS-T and one wash with TBS, secondary antibody conjugated to alkaline phosphatase (goat anti mouse IgG-AP, Sigma-Aldrich/Merck, Darmstadt, Germany, cat. no. A9316, diluted at 1:30000) was applied for 1 h. Unbound antibodies were removed by two washes with TBS-T, and membranes were equilibrated in AP buffer. Chromogenic detection was performed in 6 ml AP buffer with 21 µl NBT (75 mg ml^{-1} in 70% DMF) and 27 µl X-phosphate (50 mg ml^{-1} in 100% DMF). Reactions were stopped by addition of ddH_2O. All steps were carried out in the dark.

Protein-lipid interaction analysis by microscale thermophoresis

Microscale thermophoresis (MST) was used to quantify protein-lipid interactions (Wienken et al., 2010). Measurements were performed using a Monolith NT.115 instrument with MO.Control software (version 1.6.1; NanoTemper Technologies, Munich, Germany). Target proteins were covalently labelled with an sfGFP tag and a His_6 tag for enrichment, and protein concentrations were adjusted to yield a constant fluorescence signal. Enriched recombinant sfGFP–His_6 protein was used as a negative control. Protein dilutions were prepared in MST buffer (50 mM Tris/HCl pH 7.5, 150 mM NaCl, 0.05 % (w/v) Tween-20). Liposomes composed of 80 mol% PtdCho and 20 mol% phosphoinositides were prepared as described in (Julkowska et al., 2013). After extrusion through a polycarbonate membrane (pore size 0,2 µm), 1.5 ml MST buffer without Tween-20 was added, followed by centrifugation at 20,000g for 20 min at 22 °C. The sedimented liposomeswere resuspended in MST buffer to 3 mM total lipid concentration. For MST experiments, a serial dilution of liposomes over 16 different concentrations was prepared in MST buffer

from 3 mM down to 45.78 nM. Target protein concentration was maintained at ~40 nM. 5 µl of of target protein solution were mixed with 5 µl of ligand liposome dilutions, incubated for 10 min at RT and loaded in Monolith NT.115 standard capillaries (NanoTemper Technologies GmbH, Munich, Germany). The measurement was performed with 20 % excitation power and medium MST-Power at an ambient temperature of 22 °C. Data were analyzed with the MO. Affinity Analysis software (version v2.3., NanoTemper Technologies GmbH, Munich, Germany) using the signal from an MST-on time of 1.5 s.

Yeast-two-hybrid analysis

Protein–protein interactions were assessed using split-ubiquitin membrane-based yeast two-hybrid analysis (Dualmembrane Kit 3, Dualsystems Biotech) following established protocols (Johnsson and Varshavsky, 1994). In brief, bait constructs encoding AtPIP5K2 or AtPIP5K6 and prey with pollen-specific class VIII myosins or class XI myosins, were co-transformed into the NMY51 yeast strain (Dualsystems Biotech). For controls, the bait protein was co-transformed with either NubI fused to the ER-resident protein Alg5 (positive control) or NubG fused to Alg5 (negative control). Interaction-dependent growth was tested on selective SD medium lacking leucine, tryptophan, and histidine (SD-LWH).

Accession numbers

PIP5K2, At1g77740; *PIP5K6*, At3g07960; *ATM2*, At5g54280; *NtMyo2-like isoform X2*, LOC107765078; *VIII-B*, At4g27370; *XI-1*, At1g17580; *XI-2*, At5g43900; *XI-A*, At1g04600; *XI-C*, At1g08730; *XI-E*, At1g54560; *XI-H*, At4g28710; *XI-I*, At4g33200; *AtPTase11*, At1g47510; *SAC9*, At3g59770

Acknowledgements

We thank Dr. Mareike Heilmann for suggestions and insightful discussion. This research was supported by the German Research Foundation (DFG) through DFG grant He3424/6-2 (to I.H.), the Research Training Group RTG 2498 "Communication and Dynamics of Plant Cell Compartments" (DFG grant 400681449, project P01, to I.H.), and through the Collaborative Research Centre CRC 1664 "Plant Proteoform Diversity—SNP2Prot" (DFG grant 514901783, project B01, to I.H.).

Author Contributions

V.W., M.F., J.U., C.K., A.S., K.B., and I.H. designed research; V.W., M.F., J.U., A.S., and C.K. performed experiments; V.W., M.F., J.U., and I.H. analyzed data; V.W. and I.H. wrote the paper; V.W., M.F., J.U., A.S., C.K., K.B., and I.H. read and commented on the paper.

References

Berg, S., Kutra, D., Kroeger, T., Straehle, C.N., Kausler, B.X., Haubold, C., Schiegg, M., Ales, J., Beier, T., Rudy, M., Eren, K., Cervantes, J.I., Xu, B., Beuttenmueller, F., Wolny, A., Zhang, C., Koethe, U., Hamprecht, F.A., and Kreshuk, A. (2019). ilastik: interactive machine learning for (bio)image analysis. Nat Methods **16,** 1226–1232.

Bolte, S., and Cordelieres, F.P. (2006). A guided tour into subcellular colocalization analysis in light microscopy. J Microsc **224,** 213–232.

Braga, T., Dias, F.V., Fratini, M., Serrazina, S., Heilmann, I., and Malho, R. (2023). Functional analysis of phospholipid signaling and actin dynamics: The use of apical growing tobacco pollen tubes in a case study. Methods Mol Biol **2604,** 237–247.

Bretscher, A., Edwards, K., and Fehon, R.G. (2002). ERM proteins and merlin: integrators at the cell cortex. Nat Rev Mol Cell Biol **3,** 586–599.

Cremona, O., and De Camilli, P. (2001). Phosphoinositides in membrane traffic at the synapse. J Cell Sci **114,** 1041–1052.

Dejonghe, W., Kuenen, S., Mylle, E., Vasileva, M., Keech, O., Viotti, C., Swerts, J., Fendrych, M., Ortiz-Morea, F.A., Mishev, K., Delang, S., Scholl, S., Zarza, X., Heilmann, M., Kourelis, J., Kasprowicz, J., Nguyen le, S.L., Drozdzecki, A., Van Houtte, I., Szatmari, A.M., Majda, M., Baisa, G., Bednarek, S.Y., Robert, S., Audenaert, D., Testerink, C., Munnik, T., Van Damme, D., Heilmann, I., Schumacher, K., Winne, J., Friml, J., Verstreken, P., and Russinova, E. (2016). Mitochondrial uncouplers inhibit clathrin-mediated endocytosis largely through cytoplasmic acidification. Nat Commun **7,** 11710.

Denninger, P., Reichelt, A., Schmidt, V.A.F., Mehlhorn, D.G., Asseck, L.Y., Stanley, C.E., Keinath, N.F., Evers, J.F., Grefen, C., and Grossmann, G. (2019). Distinct RopGEFs Successively Drive Polarization and Outgrowth of Root Hairs. Curr Biol **29,** 1854–1865.

Desrivieres, S., Cooke, F.T., Parker, P.J., and Hall, M.N. (1998). MSS4, a phosphatidylinositol-4-phosphate 5-kinase required for organization of the actin cytoskeleton in Saccharomyces cerevisiae. J Biol Chem **273,** 15787–15793.

Feiguelman, G., Fu, Y., and Yalovsky, S. (2018). ROP GTPases Structure-Function and Signaling Pathways. Plant Physiol **176,** 57–79.

Franciosini, A., Rymen, B., Shibata, M., Favero, D.S., and Sugimoto, K. (2016). Molecular networks orchestrating plant cell growth. Curr Opin Plant Biol **35,** 98–104.

Fratini, M., Krishnamoorthy, P., Stenzel, I., Riechmann, M., Matzner, M., Bacia, K., Heilmann, M., and Heilmann, I. (2021). Plasma membrane nano-organization specifies phosphoinositide effects on Rho-GTPases and actin dynamics in tobacco pollen tubes. Plant Cell **33,** 642–670.

Fritz, C., Reimann, T.M., Adler, J., Knab, J., Schulmeister, S., Kriechbaum, C., Muller, S., Parmryd, I., and Kost, B. (2024). Plasma membrane and cytoplasmic compartmentalization: A dynamic structural framework required for pollen tube tip growth. Plant Physiol **197,** kiae558.

Fu, Y. (2015). The cytoskeleton in the pollen tube. Curr Opin Plant Biol **28,** 111–119.

Fukami, K., Furuhashi, K., Inagaki, M., Endo, T., Hatano, S., and Takenawa, T. (1992). Requirement of phosphatidylinositol 4,5-bisphosphate for alpha-actinin function. Nature **359,** 150–152.

Gerth, K., Lin, F., Daamen, F., Menzel, W., Heinrich, F., and Heilmann, M. (2017). Arabidopsis phosphatidylinositol 4-phosphate 5-kinase 2 contains a functional nuclear localization sequence and interacts with alpha-importins. Plant J **92,** 862–878.

Grebnev, G., Ntefidou, M., and Kost, B. (2017). Secretion and Endocytosis in Pollen Tubes: Models of Tip Growth in the Spot Light. Front Plant Sci **8,** 154.

Gungabissoon, R.A., Jiang, C.-J., Drobak, B.K., Maciver, S.K., and Hussey, P.J. (1998). Interaction of maize actin-depolymerising factor with actin and phosphoinositides and its inhibition of plant phospholipase C. Plant J **16,** 689–696.

Guo, J., and Yang, Z. (2020). Exocytosis and endocytosis: coordinating and fine-tuning the polar tip growth domain in pollen tubes. J Exp Bot **71,** 2428–2438.

Haraguchi, T., Tominaga, M., Matsumoto, R., Sato, K., Nakano, A., Yamamoto, K., and Ito, K. (2014). Molecular characterization and subcellular localization of Arabidopsis class VIII myosin, ATM1. J Biol Chem **289,** 12343–12355.

Heilmann, I., and Ischebeck, T. (2016). Male functions and malfunctions: the impact of phosphoinositides on pollen development and pollen tube growth. Plant Reprod **29,** 3–20.

Heilmann, I., Perera, I.Y., Gross, W., and Boss, W.F. (2001). Plasma membrane phosphatidylinositol 4,5-bisphosphate levels decrease with time in culture. Plant Physiol **126,** 1507–1518.

Heilmann, M., and Heilmann, I. (2025). Getting attached to membranes-How plant signaling networks employ PtdIns(4,5)P2. Plant Physiol **197**.

Hempel, F., Stenzel, I., Heilmann, M., Krishnamoorthy, P., Menzel, W., Golbik, R., Helm, S., Dobritzsch, D., Baginsky, S., Lee, J., Hoehenwarter, W., and Heilmann, I. (2017). MAPKs influence pollen

tube growth by controlling the formation of phosphatidylinositol 4,5-bisphosphate in an apical plasma membrane domain. Plant Cell **29,** 3030–3050.

Higashiyama, T., and Takeuchi, H. (2015). The mechanism and key molecules involved in pollen tube guidance. Annu Rev Plant Biol **66,** 393–413.

Hsu, S.W., Cheng, C.L., Tzen, T.C., and Wang, C.S. (2010). Rop GTPase and its target Cdc42/Rac-interactive-binding motif-containing protein genes respond to desiccation during pollen maturation. Plant Cell Physiol **51,** 1197–1209.

Im, Y.J., Davis, A.J., Perera, I.Y., Johannes, E., Allen, N.S., and Boss, W.F. (2007). The N-terminal Membrane Occupation and Recognition Nexus Domain of *Arabidopsis* Phosphatidylinositol Phosphate Kinase 1 Regulates Enzyme Activity. J Biol Chem **282,** 5443–5452.

Ischebeck, T., Stenzel, I., and Heilmann, I. (2008). Type B phosphatidylinositol-4-phosphate 5-kinases mediate pollen tube growth in *Nicotiana tabacum* and *Arabidopsis* by regulating apical pectin secretion. Plant Cell **20,** 3312–3330.

Ischebeck, T., Seiler, S., and Heilmann, I. (2010a). At the poles across kingdoms: phosphoinositides and polar tip growth. Protoplasma **240,** 13–31.

Ischebeck, T., Vu, L.H., Jin, X., Stenzel, I., Löfke, C., and Heilmann, I. (2010b). Functional cooperativity of enzymes of phosphoinositide conversion according to synergistic effects on pectin secretion in tobacco pollen tubes. Mol Plant **3,** 870–881.

Ischebeck, T., Stenzel, I., Hempel, F., Jin, X., Mosblech, A., and Heilmann, I. (2011). Phosphatidylinositol-4,5-bisphosphate influences Nt-Rac5-mediated cell expansion in pollen tubes of Nicotiana tabacum. Plant J **65,** 453–468.

Ischebeck, T., Werner, S., Krishnamoorthy, P., Lerche, J., Meijon, M., Stenzel, I., Löfke, C., Wiessner, T., Im, Y.J., Perera, I.Y., Iven, T., Feussner, I., Busch, W., Boss, W.F., Teichmann, T., Hause, B., Persson, S., and Heilmann, I. (2013). Phosphatidylinositol 4,5-bisphosphate influences PIN polarization by controlling clathrin-mediated membrane trafficking in Arabidopsis. Plant Cell **25,** 4894–4911.

Jaillais, Y., Bayer, E., Bergmann, D.C., Botella, M.A., Boutte, Y., Bozkurt, T.O., Caillaud, M.C., Germain, V., Grossmann, G., Heilmann, I., Hemsley, P.A., Kirchhelle, C., Martiniere, A., Miao, Y., Mongrand, S., Muller, S., Noack, L.C., Oda, Y., Ott, T., Pan, X., Pleskot, R., Potocky, M., Robert, S., Rodriguez, C.S., Simon-Plas, F., Russinova, E., Van Damme, D., Van Norman, J.M., Weijers, D., Yalovsky, S., Yang, Z., Zelazny, E., and Gronnier, J. (2024). Guidelines for naming and studying plasma membrane domains in plants. Nat Plants **10,** 1172–1183.

Johnsson, N., and Varshavsky, A. (1994). Split ubiquitin as a sensor of protein interactions in vivo. Proc Natl Acad Sci U S A **91,** 10340–10344.

Julkowska, M.M., Rankenberg, J.M., and Testerink, C. (2013). Liposome-binding assays to assess specificity and affinity of phospholipid-protein interactions. Methods Mol Biol **1009,** 261–271.

Kastner, C., Wagner, V.C., Fratini, M., Dobritzsch, D., Fuszard, M., Heilmann, M., and Heilmann, I. (2022). The pollen-specific class VIII-myosin ATM2 from Arabidopsis thaliana associates with the plasma membrane through a polybasic region binding anionic phospholipids. Biochimie **203,** 65–76.

Kawaguchi, K., and Asano, S. (2022). Pathophysiological Roles of Actin-Binding Scaffold Protein, Ezrin. Int J Mol Sci **23**.

Klahre, U., and Kost, B. (2006). Tobacco RhoGTPase ACTIVATING PROTEIN1 spatially restricts signaling of RAC/Rop to the apex of pollen tubes. Plant Cell **18,** 3033–3046.

Klahre, U., Becker, C., Schmitt, A.C., and Kost, B. (2006). Nt-RhoGDI2 regulates Rac/Rop signaling and polar cell growth in tobacco pollen tubes. Plant J **46,** 1018–1031.

König, S., Ischebeck, T., Lerche, J., Stenzel, I., and Heilmann, I. (2008). Salt stress-induced association of phosphatidylinositol-4,5-bisphosphate with clathrin-coated vesicles in plants. Biochem J **415,** 387–399.

Kost, B. (2008). Spatial control of Rho (Rac-Rop) signaling in tip-growing plant cells. Trends Cell Biol **18,** 119–127.

Kost, B., Spielhofer, P., and Chua, N.H. (1998). A GFP-mouse talin fusion protein labels plant actin filaments in vivo and visualizes the actin cytoskeleton in growing pollen tubes. Plant J **16,** 393–401.

Kost, B., Lemichez, E., Spielhofer, P., Hong, Y., Tolias, K., Carpenter, C., and Chua, N.H. (1999). Rac homologues and compartmentalized phosphatidylinositol 4, 5-bisphosphate act in a common pathway to regulate polar pollen tube growth. J Cell Biol **145,** 317–330.

Lacalle, R.A., Peregil, R.M., Albar, J.P., Merino, E., Martinez, A.C., Merida, I., and Manes, S. (2007). Type I phosphatidylinositol 4-phosphate 5-kinase controls neutrophil polarity and directional movement. J Cell Biol.

Lebecq, A., Doumane, M., Fangain, A., Bayle, V., Leong, J.X., Rozier, F., Marques-Bueno, M.D., Armengot, L., Boisseau, R., Simon, M.L., Franz-Wachtel, M., Macek, B., Ustun, S., Jaillais, Y., and Caillaud, M.C. (2022). The Arabidopsis SAC9 enzyme is enriched in a cortical population of early endosomes and restricts PI(4,5)P(2) at the plasma membrane. Elife **11**.

Lord, E.M., and Russell, S.D. (2002). The mechanisms of pollination and fertilization in plants. Annu Rev Cell Dev Biol **18,** 81–105.

Menzel, W., Stenzel, I., Helbig, L.M., Krishnamoorthy, P., Neumann, S., Eschen-Lippold, L., Heilmann, M., Lee, J., and Heilmann, I. (2019). A PAMP-triggered MAPK cascade inhibits phosphatidylinositol 4,5-bisphosphate production by PIP5K6 in Arabidopsis thaliana. New Phytol **224,** 833–847.

Muller, M., and Schmidt, W. (2004). Environmentally induced plasticity of root hair development in Arabidopsis. Plant Physiol **134,** 409–419.

Nebenfuhr, A., and Dixit, R. (2018). Kinesins and Myosins: Molecular Motors that Coordinate Cellular Functions in Plants. Annu Rev Plant Biol **69,** 329–361.

Neisch, A.L., and Fehon, R.G. (2011). Ezrin, Radixin and Moesin: key regulators of membrane-cortex interactions and signaling. Curr Opin Cell Biol **23,** 377–382.

Olatunji, D., Clark, N.M., and Kelley, D.R. (2023). The class VIII myosin ATM1 is required for root apical meristem function. Development **150,** dev201762.

Orr, R.G., Cheng, X., Vidali, L., and Bezanilla, M. (2020). Orchestrating cell morphology from the inside out - using polarized cell expansion in plants as a model. Curr Opin Cell Biol **62,** 46–53.

Rausche, J., Stenzel, I., Stauder, R., Fratini, M., Trujillo, M., Heilmann, I., and Rosahl, S. (2021). A phosphoinositide 5-phosphatase from Solanum tuberosum is activated by PAMP-treatment and may antagonize phosphatidylinositol 4,5-bisphosphate at Phytophthora infestans infection sites. New Phytol **229,** 469–487.

Riedl, J., Crevenna, A.H., Kessenbrock, K., Yu, J.H., Neukirchen, D., Bista, M., Bradke, F., Jenne, D., Holak, T.A., Werb, Z., Sixt, M., and Wedlich-Soldner, R. (2008). Lifeact: a versatile marker to visualize F-actin. Nat Methods **5,** 605–607.

Rivera, G.M., Vasilescu, D., Papayannopoulos, V., Lim, W.A., and Mayer, B.J. (2009). A reciprocal interdependence between Nck and PI(4,5)P(2) promotes localized N-WASp-mediated actin polymerization in living cells. Mol Cell **36,** 525–535.

Saake, P., Brands, M., Endeshaw, A.B., Stolze, S.C., Westhoff, P., Balcke, G.U., Hensel, G., Holton, N., Zipfel, C., Tissier, A., Nakagami, H., and Zuccaro, A. (2025). Ergosterol-induced immune response in barley involves phosphorylation of phosphatidylinositol phosphate metabolic enzymes and activation of diterpene biosynthesis. New Phytol **246,** 1236–1255.

Samaj, J., Muller, J., Beck, M., Bohm, N., and Menzel, D. (2006). Vesicular trafficking, cytoskeleton and signalling in root hairs and pollen tubes. Trends Plant Sci **11,** 594–600.

Sattarzadeh, A., Franzen, R., and Schmelzer, E. (2008). The Arabidopsis class VIII myosin ATM2 is involved in endocytosis. Cell Motil Cytoskeleton **65,** 457–468.

Schindelin, J., Arganda-Carreras, I., Frise, E., Kaynig, V., Longair, M., Pietzsch, T., Preibisch, S., Rueden, C., Saalfeld, S., Schmid, B., Tinevez, J.Y., White, D.J., Hartenstein, V., Eliceiri, K., Tomancak, P., and Cardona, A. (2012). Fiji: an open-source platform for biological-image analysis. Nat Methods **9,** 676–682.

Sousa, E., Kost, B., and Malho, R. (2008). *Arabidopsis* Phosphatidylinositol-4-Monophosphate 5-Kinase 4 Regulates Pollen Tube Growth and Polarity by Modulating Membrane Recycling. Plant Cell **20,** 3050–3064.

Sparks, R.P., and Fratti, R. (2019). Use of Microscale Thermophoresis (MST) to Measure Binding Affinities of Components of the Fusion Machinery. Methods Mol Biol **1860,** 191–198.

Stenzel, I., Ischebeck, T., Quint, M., and Heilmann, I. (2012). Variable regions of PI4P 5-kinases direct PtdIns(4,5)P2 toward alternative regulatory functions in tobacco pollen tubes. Frontiers in Plant Science **2,** 1–14.

Stenzel, I., Ischebeck, T., König, S., Holubowska, A., Sporysz, M., Hause, B., and Heilmann, I. (2008). The type B phosphatidylinositol-4-phosphate 5-kinase 3 is essential for root hair formation in *Arabidopsis thaliana*. Plant Cell **20,** 124–141.

Stenzel, I., Ischebeck, T., Vu-Becker, L.H., Riechmann, M., Krishnamoorthy, P., Fratini, M., and Heilmann, I. (2020). Coordinated localization and antagonistic function of NtPLC3 and PI4P 5-kinases in the subapical plasma membrane of tobacco pollen tubes. Plants **9,** 452.

Sun, J., Eklund, D.M., Montes-Rodriguez, A., and Kost, B. (2015). In vivo Rac/Rop localization as well as interaction with RhoGAP and RhoGDI in tobacco pollen tubes: analysis by low-level expression of fluorescent fusion proteins and bimolecular fluorescence complementation. Plant J **84,** 83–98.

Tinevez, J.-Y., Perry, N., Schindelin, J., Hoopes, G.M., Reynolds, G.D., Laplantine, E., Bednarek, S.Y., Shorte, S.L., and Eliceiri, K.W. (2017). TrackMate: An open and extensible platform for single-particle tracking. Methods **115,** 80–90.

Williams, M.E., Torabinejad, J., Cohick, E., Parker, K., Drake, E.J., Thompson, J.E., Hortter, M., and Dewald, D.B. (2005). Mutations in the *Arabidopsis* phosphoinositide phosphatase gene *SAC9* lead to overaccumulation of PtdIns(4,5)P_2 and constitutive expression of the stress-response pathway. Plant Physiol **138,** 686–700.

Wu, G., Gu, Y., Li, S., and Yang, Z. (2001). A genome-wide analysis of Arabidopsis Rop-interactive CRIB motif-containing proteins that act as Rop GTPase targets. Plant Cell **13,** 2841–2856.

Wu, S.Z., and Bezanilla, M. (2014). Myosin VIII associates with microtubule ends and together with actin plays a role in guiding plant cell division. Elife **3,** 327–340.

Wu, S.Z., and Bezanilla, M. (2018). Actin and microtubule cross talk mediates persistent polarized growth. J Cell Biol **217,** 3531–3544.

Yalovsky, S., Bloch, D., Sorek, N., and Kost, B. (2008). Regulation of membrane trafficking, cytoskeleton dynamics, and cell polarity by ROP/RAC GTPases. Plant Physiol **147,** 1527–1543.

Yamamoto, M., Hilgemann, D.H., Feng, S., Bito, H., Ishihara, H., Shibasaki, Y., and Yin, H.L. (2001). Phosphatidylinositol 4,5-bisphosphate induces actin stress-fiber formation and inhibits membrane ruffling in CV1 cells. J Cell Biol **152,** 867–876.

Zhao, Y., Yan, A., Feijo, J.A., Furutani, M., Takenawa, T., Hwang, I., Fu, Y., and Yang, Z. (2010). Phosphoinositides regulate clathrin-dependent endocytosis at the tip of pollen tubes in Arabidopsis and tobacco. Plant Cell **22,** 4031–4044.

Zonia, L., and Munnik, T. (2008). Vesicle trafficking dynamics and visualization of zones of exocytosis and endocytosis in tobacco pollen tubes. J Exp Bot **59,** 861–873.

Figure Legends

Figure 1. The PtdIns(4,5)P_2 biosensor RedStar-PH_{PLC} and EYFP-ATM2 occupy overlapping subapical plasma membrane domains of tobacco pollen tubes, coinciding with actin-plasma membrane contacts.

The subcellular distribution patterns of the PtdIns(4,5)P_2 biosensor, RedStar-PH_{PLC}, EYFP-ATM2 or the PtdIns(4,5)P_2-forming enzyme, PIP5K2-EYFP, were analyzed by spinning disc microscopy (SD) or laser-scanning confocal microscopy (LSM) upon coexpression in tobacco (*N. tabacum*) pollen tubes, relative to fluorescent markers for actin (LifeAct-RFP or mTalin-YFP). Expression was driven by a pLat52 promoter.

(**A**) Fluorescence distribution of RedStar-PH_{PLC}, EYFP-ATM2 and LifeAct-RFP, as indicated, recorded by SD. Left panels, RedStar-PH_{PLC} (maximum intensity z-projection or median plane, as indicated). Right panels, EYFP-ATM2 coexpressed with LifeAct-RFP. The clear zone, the shank region, and the transition zone are indicated. Scale bars, 5 µm. Images are representative for at least three independent experiments.

(**B**) Coexpression of Arabidopsis PIP5K2-EYFP and LifeAct-RFP. Panels from left to right depict the maximum intensity z-projection from the pollen tube tip, substacks of the surface and tip periphery, the overlap regions (yellow/white) between LifeAct-RFP–marked actin filaments and AtPIP5K2-EYFP nanodomains as detected by Fiji, and a detail view (white box), highlighting actin attachment to plasma membrane nanodomains occupied by PIP5K2-EYFP (arrowheads). Scale bar, 5 µm. Images are representative for at least three independent experiments.

(**C**) Coexpression of mC-ATM2 or its tobacco homologue, mC-NtMyo2-like, with mTalin-YFP, imaged by LSM. Upper panels, merged maximum intensity z-projections; lower panels, details (white boxes) of locally increased mTalin-YFP signals at the plasma membrane (arrowheads). Scale bar, 5 µm. Images are representative for at least three independent experiments.

Figure 2. Overexpression of ATM2 stabilizes actin dynamics and induces tip swelling morphology in pollen tube cells.

Distribution and motility of the actin cytoskeleton were monitored by laser-scanning confocal microscopy (LSM) in tobacco (*N. tabacum*) pollen tubes coexpressing the actin marker, mTalin-YFP, with either an mCherry (mC)-control, or with mC-tagged variants of ATM2, including full length ATM2 (mC-ATM2), an ATM2 variant lacking the C-terminal lipid-binding region (mC-$ATM2_{\Delta LB}$), or an ATM2 variant lacking N-terminal actin-binding and protein-interaction regions (mC-$ATM2_{CT}$). Expression was driven by a pLat52 promoter.

(**A**) Schematic representation of the ATM2 protein (left) and of the mC-fusions of ATM2 variants used (right panel). Numbers indicate ATM2 residue positions. C, C-terminus; CT, C-terminal domain; IQ, calmodulin-binding IQ-motif-domain; Motor, motor-ATPase domain; N, N-terminus; NT, N-terminal domain; SH3, SRC-homology 3-domain

(**B**) To capture actin dynamics, Z-stacks (2 µm steps) were acquired in 10 s intervals over 5 min. Left column, representative maximum intensity projections of merged mTalin-YFP and mCherry fluorescence channels. Mid and right column, separate Z-projection images of the YFP channel (mTalin) or the mCherry channel (control and ATM2 variants), respectively. Arrowheads, Locally increased mTalin-YFP signal at the plasma

membrane. Scale bars, 10 µm. Right panels, Kymographs extracted from the pollen tube tip regions. Stabilized actin filaments are represented by horizontal lines.

(**C**) Degree of plasma membrane association of mC-ATM2 or the lipid-binding deficient mC-ATM2$_{\Delta LB}$ variant according to the fluorescence intensity ratio of mC signals at the plasma membrane vs. cytosol, as indicated. Data represent observations from 12 cells (mC-ATM2) or 13 cells (mC-ATM2$_{\Delta LB}$), respectively.

(**D-F**) Pollen tube cells coexpressing the actin marker mTalin-YFP with an mC-control, mC-ATM2, with mC-ATM2$_{\Delta LB}$, or with mC-ATM2$_{CT}$ were analyzed for cell morphology (**D**), actin occupancy in the cell apex (**E**), or for mean actin lifetime (**F**).

(**D**) Pollen tube tip width (in µm) determined from brightfield images using Fiji. Data represent observations from 29 cells (mC); 18 cells (mC-ATM2); 13 cells (mC-ATM2$_{\Delta LB}$); or 14 cells (mC-ATM2$_{CT}$), respectively.

(**E**) The tip actin occupancy quantified as the relative area covered by mTalin-YFP signal at the pollen tube tip. Data represent observations from 25 cells (mC); 18 cells (mC-ATM2); 16 cells (mC-ATM2$_{\Delta LB}$); or 14 cells (mC-ATM2$_{CT}$), respectively.

(**F**) Mean lifetime (in min) of mTalin-labeled actin filaments, calculated from kymographs. Data represent observations from 20 cells (mC); 18 cells (mC-ATM2); 13 cells (mC-ATM2$_{\Delta LB}$); or 14 cells (mC-ATM2$_{CT}$), respectively.

Data in (**C-F**) represents 3-4 independent experiments. Statistical differences were assessed by one-way ANOVA followed by Tukey's post-hoc test; letters denote categories of values exhibiting statistical significant differences ($p < 0.05$).

Figure 3. Artificial PtdIns(4,5)P$_2$ depletion in the plasma membrane abolishes ATM2 effects on actin dynamics.

Effects of altered plasma membrane PtdIns(4,5)P$_2$ abundance on the function of ATM2 were studied for pollen tubes coexpressing CFP-ATM2 either with an mC control, or with the PtdIns(4,5)P$_2$-specific 5-phosphatase, mC-AtPTase11, an enzyme converting PtdIns(4,5)P$_2$ to PtdIns4P. Transgenic pollen tube cells were then analyzed for cell morphology, tip actin occupancy or mean actin lifetime. Expression was driven by a Lat52 promoter.

(**A**) Representative fluorescence images of pollen tubes coexpressing mTalin-YFP with CFP-ATM2 and either an mC control (upper panels) or with mC-AtPTase11 (lower panels), as indicated. Individual fluorescence channels and merged images, as indicated. Scale bars, 5 µm.

(**B**) Degree of plasma membrane association of CFP-ATM2 in control cells coexpressing mC or in cells coexpressing mC-PTase11 according to the fluorescence intensity ratio of mC signals at the plasma membrane vs. cytosol. Data represent observations from 12 cells (mC) or 12 cells (mC-PTase11), respectively.

(**C**) Pollen tube tip with in µm (left panel), apical actin occupancy (mid panel), or mean actin lifetime in min (right panel) of mTalin-YFP-labeled actin filaments, as indicated. Data represent observations from 20-29 cells (mC-control); 6 cells (CFP-ATM2 plus mC); or 15 cells (mC-AtPTase11), respectively. Data were collected from at least three independent experiments.

(**D**) The mean actin lifetime of plasma membrane-proximal actin decorated by mTalin-YFP was recorded by acquiring kymographs along the plasma membrane periphery of the cell apex (yellow line). Images (left panels) are illustrating the analysis done. Right panel, Plasma membrane-peripheral mean actin lifetime for control pollen tubes expressing only mC, or for cells coexpressing CFP-ATM2 either with an mC control, or with mC-AtPTase11, as indicated. Data represent observations from 6 cells (mC-control); 8 cells (CFP-ATM2 plus mC); or 7 cells (mC-AtPTase11), respectively. Data were collected from at least three independent experiments.

Statistical differences were assessed by one-way ANOVA followed by Tukey's post-hoc test; letters denote categories of values exhibiting statistical significant differences ($p < 0.05$).

Figure 4. Lipid-binding features of recombinant C-terminal ATM2 fragments.

Lipid binding of the polybasic C-terminal region of ATM2 was revisited by biochemical analysis, including quantitative MST-analysis. ATM2-variants representing the C-terminal region of ATM2 ($ATM2_{CT}$, residues 972-1220,) or the derived lipid binding-deficient variant $ATM2_{CT\Delta LB}$ (residues 972-1177) were recombinantly expressed as fusions to C-terminal His_6-tags, enriched, and used for *in vitro* protein-lipid interaction tests. For MST-analysis, protein were additionally fused to N-terminal superfolder (sf)GFP-tags. Enriched sfGFP or MBP alone were used as negative controls, respectively.

(**A**) Protein-lipid overlay assay for binding of a MBP-His_6 control, $ATM2_{CT}$-His_6 or $ATM2_{CT\Delta LB}$-His_6 to phospholipids (10 nmol) using commercial PIP strips (Echelon Biosciences Inc.). Images of the developed protein-lipid overlay blots are representative for three experiments.

(**B**) Exemplary Coomassie blue-stained SDS-PAGE gel of enriched recombinant sfGFP-fusions used for lipid-binding tests by MST, as indicated. Deduced fragment masses: sfGFP-His_6, 28.5 kDa; sfGFP-$ATM2_{CT}$-His_6, 57.6 kDa; sfGFP-$ATM2_{CT\Delta LB}$-His_6, 52.4 kDa.

(**C**) MST-analysis of the binding of enriched sfGFP–$ATM2_{CT}$-His_6 to DOPC-liposomes containing 20 mol% PtdIns(4,5)P_2 (green) or 20 mol% PtdIns4P (blue). Binding curves depict the fraction of bound protein plotted versus the logarithmic ligand concentration. Proteins were incubated at an approx. concentration of 40 nM with liposomes serially diluted from 45.78 nM - 3 mM total lipid over 16 dilution steps. The MST-on time was 2.5 s; data were fitted with the KD-fit model. Each point represents four independent measurements; error bars indicate standard deviation.

(**D**) MST control-measurements with enriched sfGFP-His_6 and DOPC-liposomes containing 20 mol% PtdIns(4,5)P_2 (green) or 20 mol% PtdIns4P (blue). As no binding was detected for sfGFP-His_6, data is represented as Fnorm in ‰ against the logarithmic ligand concentration.

(**E**) MST-analysis comparing the binding of enriched $ATM2_{CT}$ (dark green), $ATM2_{CT\Delta LB}$-His_6 (light green) or sfGFP-His_6 (brown) to DOPC-liposomes containing 20 mol% PtdIns(4,5)P_2. MST-on time was 2.5 s and data were fitted using the KD-fit model. Each data point represents four independent measurements with error bars indicating standard deviation. $ATM2_{CT}$ data are same as in (**C**).

(**F**) KD values representing binding affinities for measurements presented in (**C**) or (**E**). Signal to noise ratios (not shown) were above 5, reflecting reliable binding measurements. Relative affinities are given for binding to PtdIns(4,5)P_2-containing liposomes as a reference (right column).

Figure 5. ATM2-EYFP colocalizes with RedStar-PH_{PLC} in plasma membrane nanodomains and promotes PtdIns(4,5)P_2 formation by PIP5K2 *in vivo* and *in vitro*.

The functional interplay of ATM2 with PtdIns(4,5)P_2 or PIP5K2 was analyzed in more detail by *in vivo* and *in vitro* experiments.

(**A**) Fluorescence distribution of ATM2-EYFP and the coexpressed PtdIns(4,5)P_2 biosensor, RedStar-PH_{PLC} in tobacco pollen tubes, visualized by spinning disc microscopy (SD). Images represent maximum intensity projections from z-stacks acquired in 0.3 µm slices. Upper panels, 3D projections of the EYFP channel (left), RedStar channel (mid), and the merged image (right). Scale bar, 5 µm. Lower panels, magnified regions of interest (white boxes). Scale bars, 1 µm. Right panels, Fluorescence intensity plots for the EYFP and RedStar channels, recorded along the dashed line. Mander's colocalization coefficients were calculated for fluorescent nanodomains in red → green and in green → red directions, as indicated.

(**B**) Spatial extent of the subapical plasma membrane domain decorated by RedStar-PH_{PLC} upon coexpression with a EYFP-control (left panel), with ATM2-EYFP (mid panel), or with $ATM2_{\Delta LB}$-EYFP (right panel), as indicated. Upper panels show representative images, respectively. Please note the loss of plasma membrane association for $ATM2_{\Delta LB}$-EYFP. Arrows indicate the extent of the RedStar-PH_{PLC}-labeled membrane domain as maximum didtance from apex. Lower panels, Spatial extent of the plasma membrane domain labeled by RedStar-PH_{PLC} upon coexpression with the EYFP-control, with ATM2-EYFP, or with $ATM2_{\Delta LB}$-EYFP, as indicated (left). The area density of punctate signals decorated by RedStar-PH_{PLC} was analyzed for pollen tubes expressing the EYFP-control, ATM2-EYFP, or $ATM2_{\Delta LB}$-EYFP, as indicated (right). Data represent observations from 8 cells (EYFP-control); 14 cells (ATM2-EYFP); or 9 cells (ATM2-$EYFP_{\Delta LB}$), respectively. Statistical differences were assessed by one-way ANOVA followed by Tukey's post-hoc test; letters denote categories of values exhibiting statistical significant differences ($p < 0.05$).

(**C**) Yeast-two-hybrid analysis using PIP5K2 or PIP5K6, respectively, as bait proteins against selected myosin isoforms, including the pollen-specific class VIII myosins ATM2 or VIIIB, and various class XI myosins, as indicated. Left panels, interaction tests with PIP5K2 as a bait; right panels, interactions tests with PIP5K6 as a bait. Yeast growth on non-selective SD–LW medium confirmed correct transformation, while growth on selective SD–LWH medium indicated positive interactions. Results are representative for three independent biological replicates, each performed in triplicates.

(**D**) Enriched recombinant MBP-PIP5K2 fusion protein expressed in *E. coli* was tested for *in vitro* catalytic activity, converting PtdIns4P to PtdIns(4,5)P_2 in the presence of [γ-^{32}P]ATP. Formation of radiolabeled PtdIns(4,5)P_2 was monitored by phosphormaging after chromatographic separation of the reaction products. Assays were performed with *E. coli* extract as a negative control, with MBP-PIP5K2 alone, or upon coincubation of MBP-PIP5K2 with enriched recombinant C-terminal fragments of the class VIII-myosins, VIII-B or ATM2, as indicated. The image shows a representative phosphorimage. The experiment was performed five times with similar results.

(**E**) Quantification of PtdIns(4,5)P_2 production from assays shown in (**D**), reported in relative units. Additional controls include coincubation of MBP-PIP5K2 with the small GTPase ROP2 (a PtdIns(4,5)P_2-binding protein) and its constitutively active (G15V) or dominant-negative (T20N) variants, as indicated. Asterisks indicate statistical differences from the MBP-PIP5K2 control, according to a Student's *t*-test ($p < 0.05$). n.s., not significant.

Figure 6. Effects of ATM2 are influenced by coexpression of NtRhoGDI2.

The guanine-nucleotide dissociation inhibitor, NtRhoGDI2, was previously shown to counteract PIP5K2/PtdIns(4,5)P_2-dependent stabilization of actin dynamics in pollen tubes. The influence of NtRhoGDI2 on ATM2-mediated effects was analyzed by protein-protein interaction studies, by coexpression of fluorescent protein fusions in tobacco pollen tubes, and by assessing pollen tube cell morphology.

(**A**) Yeast-two-hybrid analysis using PIP5K2 or ATM2, respectively, as bait proteins against NtRhoGDI2. Left, interaction tests with PIP5K2 as a bait; right, interactions tests with ATM2 as a bait. Yeast growth on non-selective SD–LW medium confirmed correct transformation, while growth on selective SD–LWH medium indicated positive interactions. Results are representative for three independent biological replicates, each performed in triplicates.

(**B**) Representative confocal images of tobacco pollen tubes coexpressing mC-ATM2 with either EYFP (top) or with NtRhoGDI2-EYFP (bottom), as indicated. Scale bars, 5 µm.

(**C**) Spatial distribution of mC-ATM2 mean normalized fluorescence intensity (±SEM) along the plasma membrane, plotted as mean normalized intensity (AU) against the distance from the apex (µm) for mC-ATM2 coexpressed with EYFP (green) or with NtRhoGDI2-EYFP (orange). The dashed line indicates the threshold of 0.25 intensity units used for domain signal length estimation. Data represent observations from 10 cells (EYFP) or 18 cells (NtRhoGDI2-EYFP), respectively, from two independent experiments.

(**D**) Dimension of the plasma membrane domain decorated by mC-ATM2 above the 0.25 threshold in pollen tubes coexpressing mC-ATM2 with either EYFP or with NtRhoGDI2-EYFP, as indicated. Data represent 2-3 independent experiments. The asterisk indicates a significantly difference according to a Student's *t*-test ($p < 0.05$).

(**E**) Mean normalized fluorescence intensity of mC-ATM2 coexpressed with EYFP (white) or with NtRhoGDI2-EYFP (grey), in the tip (0-20 µm distance from apex) or shank regions (20-40 µm distance from apex) of the pollen tube cells. Data represent 2-3 independent experiments. Statistical differences were

determined by one-way ANOVA followed by Tukey's post-hoc test; letters denote categories of values exhibiting statistical significant differences ($p < 0.05$).

(**F**) Pollen tube tip with in µm of pollen tubes coexpressing ATM2-MC with EYFP or with NtRhoGDI2-EYFP, as indicated. Data represents two independent experiments. The asterisk indicates a significantly difference according to a Student's *t*-test ($p < 0.001$).

Figure 7. Simplified schematic of ATM2-mediated activation of PIP5K2, locally potentiating PtdIns(4,5)P_2 production at the actin-plasma membrane interface.

The class VIII myosin ATM2 forms an interface between actin filaments and the plasma membrane by binding to anionic phospholipid headgroups and to actin filaments. ATM2 might at least transiently occur in complex with PIP5K2 and NtRhoGDI2. By binding to ATM2, catalytic activity of PIP5K2 is enhanced, thereby promoting PtdIns(4,5)P_2 formation at actin-plasma membrane contact sites. The locally increased abundance of PtdIns(4,5)P_2 acts as a positional signal for the recruitment of further ATM2 proteins, and acts as a GDF on NtRhoGDI2, mediating enhanced activation of Rac/ROP proteins, to facilitate actin stabilization. Alternative explanations are possible. GDF, guanine nucleotide displacement factor; PtdIns4P, phosphatidylinositol 4-phosphate; PtdIns(4,5)P_2, phosphatidylinositol 4,5-bisphosphate

Supplemental Figure 1. Relaxed localization of AtPIP5K2$_{344-754}$-EYFP in a plasma membrane-peripheral network-like pattern in tobacco pollen tubes.

The fluorescence distribution of AtPIP5K2-EYFP or the N-terminally truncated AtPIP5K2$_{344-754}$-EYFP was analyzed by spinning disc microscopy upon transient expression in tobacco pollen tubes.

Top panel, Representation of the expressed EYFP fusion proteins. NT, N-terminal domain; MORN, membrane occupation and recognition nexus repeat domain; Lin, hypervariable linker region; Dim, dimerization domain; Cat, catalytic domain; AL, activation loop

Bottom panels, AtPIP5K2-EYFP displays dot-like plasma membrane association resembling nanodomains in the apex of a tobacco pollen tube (left). AtPIP5K2$_{344-754}$-EYFP decorates a plasma membrane-proximal filamentous network-pattern, possibly representing the cortical actin network. Images are representative for three independent experiments.

Supplemental Figure 2. Detailed analysis of mean actin lifetimes in pollen tube cells expressing an mC-control, mC-ATM2, or mC-ATM2$_{\Delta LB}$.

Data from the analysis of mean lifetimes of mTalin-labeled actin filaments were calculated from kymographs and analyzed for the proportion of filaments displaying low-mobility.

(**A**) Proportion of mTalin-YFP sigbals displaying a spatial persistence of 0 min - 1 min (grey, high mobility) or of 1 min - 5 min (black, low mobility).

(**B**) Exact number underlying the representation in (**A**). Data represent observations from 20 cells (mC); 18 cells (mC-ATM2); 13 cells (mC-ATM2$_{\Delta LB}$); or 14 cells (mC-ATM2$_{CT}$), respectively.

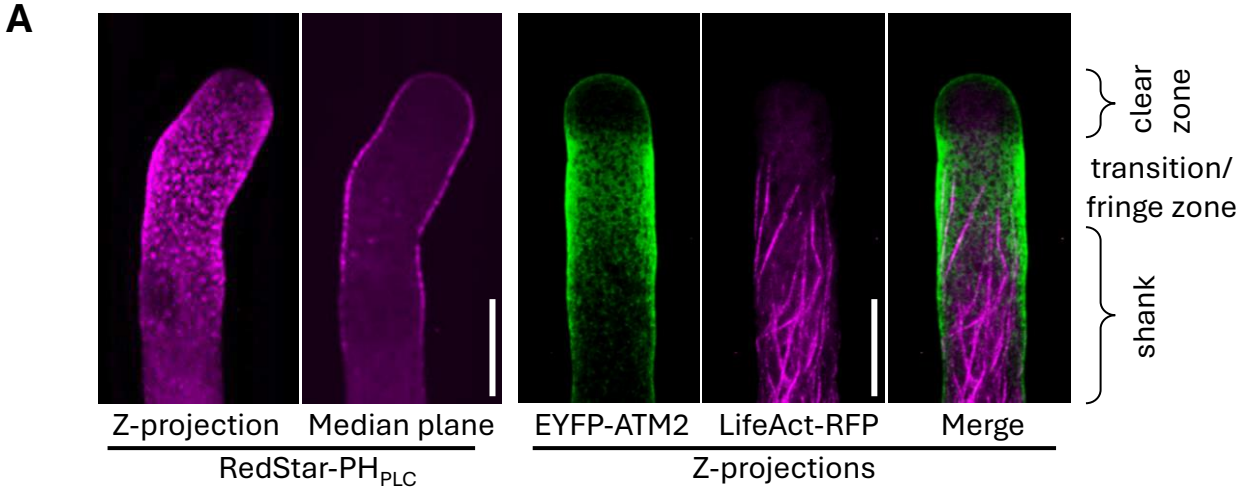
Supplemental Figure 3. Artificial PtdIns(4,5)P$_2$ depletion in the plasma membrane abolishes ATM2 effects on actin dynamics.

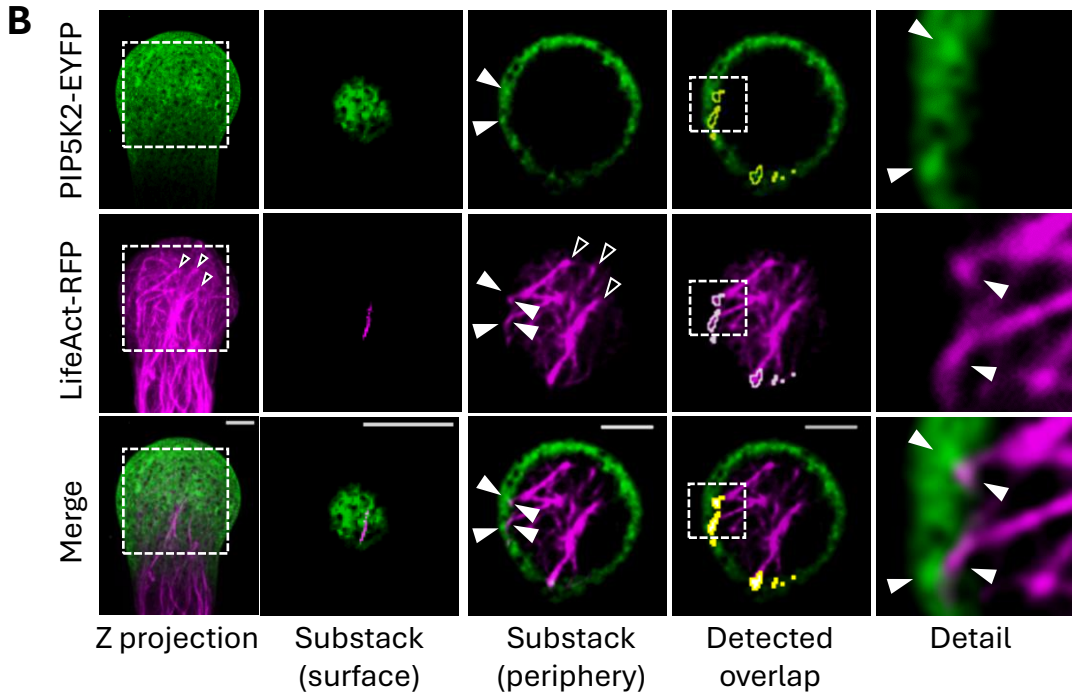
Effects of altered plasma membrane PtdIns(4,5)P$_2$ abundance on the function of ATM2 were studied for pollen tubes coexpressing CFP-ATM2 either with an mC control, or with the PtdIns(4,5)P$_2$-specific 5-phosphatase, SAC9, an enzyme converting PtdIns(4,5)P$_2$ to PtdIns4P. Transgenic pollen tube cells were then analyzed for cell morphology or mean actin lifetime. Expression was driven by a Lat52 promoter.

(**A**) Actin occupancy in the cell apex was determined for cells expressing fluorescent fusion proteins, as indicated. Data were collected from at least three independent experiments (mC-control, 25 cells; CFP-ATM2, 6 cells; SAC9, 25 cells).

(**B**) Mean actin lifetime of mTalin-YFP signals was recorded by acquiring kymographs. Data were collected from at least three independent experiments (mC-control, 20 cells; CFP-ATM2, 6 cells; SAC9, 25 cells).

Statistical differences were assessed by one-way ANOVA followed by Tukey's post-hoc test; letters denote categories of values exhibiting statistical significant differences ($p < 0.05$).


A
clear zone
transition/ fringe zone
shank
Z-projection
Median plane
EYFP-ATM2
LifeAct-RFP
Merge
RedStar-PH$_{PLC}$
Z-projections


B
PIP5K2-EYFP
LifeAct-RFP
Merge
Z projection
Substack (surface)
Substack (periphery)
Detected overlap
Detail

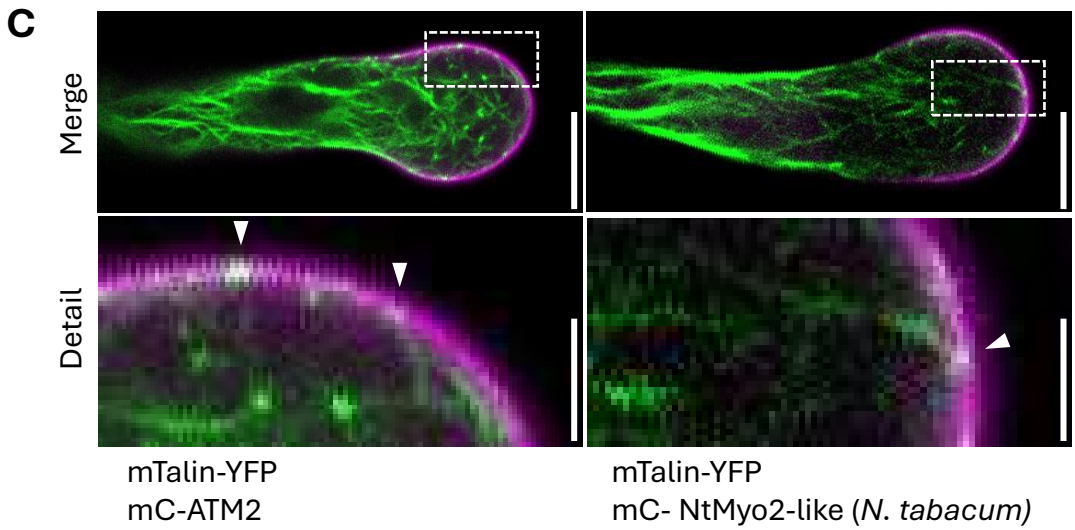

C
Merge
Detail
mTalin-YFP
mC-ATM2
mTalin-YFP
mC- NtMyo2-like (N. tabacum)

Figure 1

Figure 1. The PtdIns(4,5)P_2 biosensor RedStar-PH_{PLC} and EYFP-ATM2 occupy overlapping subapical plasma membrane domains of tobacco pollen tubes, coinciding with actin-plasma membrane contacts.

The subcellular distribution patterns of the PtdIns(4,5)P_2 biosensor, RedStar-PH_{PLC}, EYFP-ATM2 or the PtdIns(4,5)P_2-forming enzyme, PIP5K2-EYFP, were analyzed by spinning disc microscopy (SD) or laser-scanning confocal microscopy (LSM) upon coexpression in tobacco (*N. tabacum*) pollen tubes, relative to fluorescent markers for actin (LifeAct-RFP or mTalin-YFP). Expression was driven by a pLat52 promoter.

(**A**) Fluorescence distribution of RedStar-PH_{PLC}, EYFP-ATM2 and LifeAct-RFP, as indicated, recorded by SD. Left panels, RedStar-PH_{PLC} (maximum intensity z-projection or median plane, as indicated). Right panels, EYFP-ATM2 coexpressed with LifeAct-RFP. The clear zone, the shank region, and the transition zone are indicated. Scale bars, 5 µm. Images are representative for at least three independent experiments.

(**B**) Coexpression of Arabidopsis PIP5K2-EYFP and LifeAct-RFP. Panels from left to right depict the maximum intensity z-projection from the pollen tube tip, substacks of the surface and tip periphery, the overlap regions (yellow/white) between LifeAct-RFP–marked actin filaments and AtPIP5K2-EYFP nanodomains as detected by Fiji, and a detail view (white box), highlighting actin attachment to plasma membrane nanodomains occupied by PIP5K2-EYFP (arrowheads). Scale bar, 5 µm. Images are representative for at least three independent experiments.

(**C**) Coexpression of mC-ATM2 or its tobacco homologue, mC-NtMyo2-like, with mTalin-YFP, imaged by LSM. Upper panels, merged maximum intensity z-projections; lower panels, details (white boxes) of locally increased mTalin-YFP signals at the plasma membrane (arrowheads). Scale bar, 5 µm. Images are representative for at least three independent experiments.

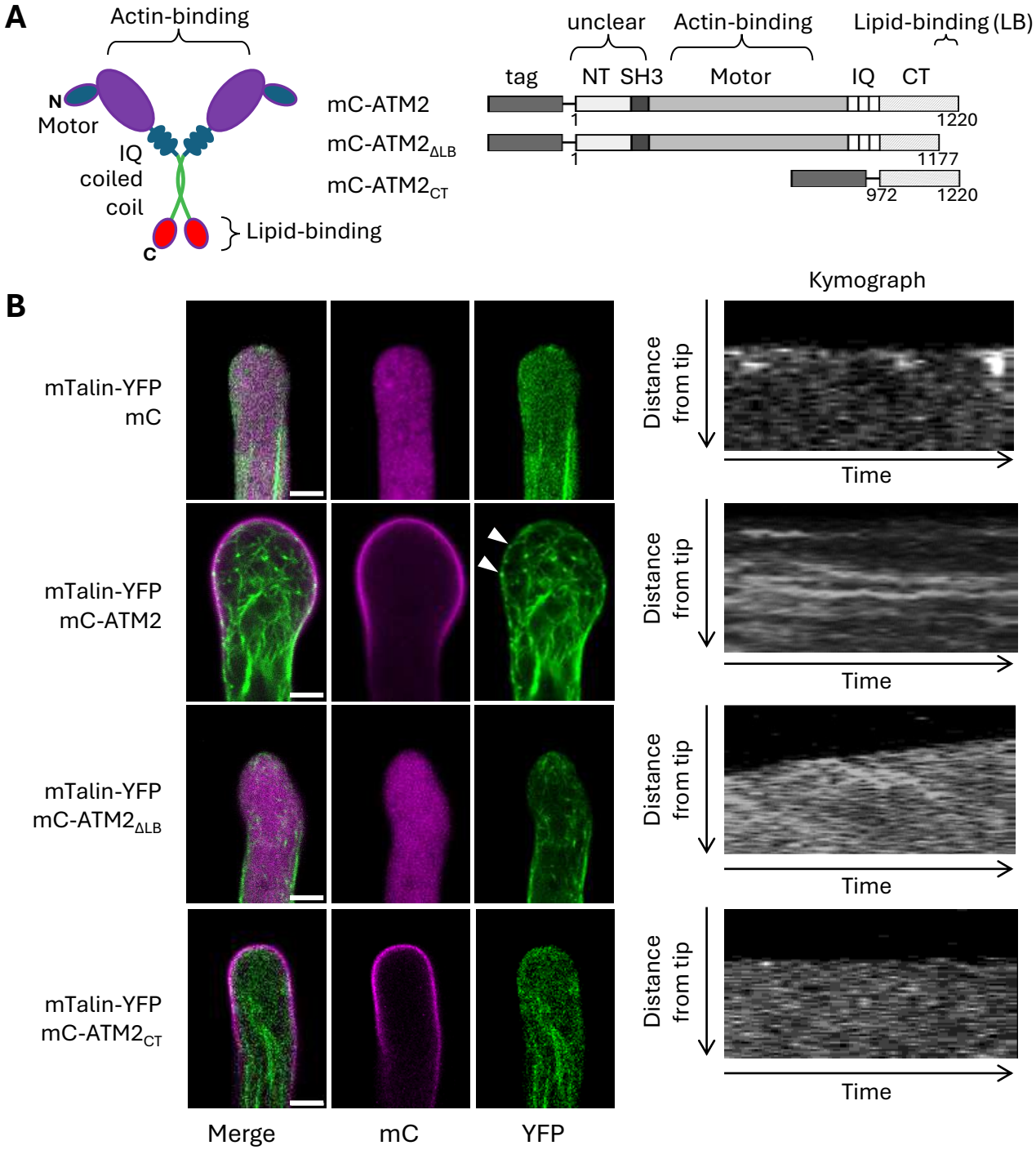

A
Actin-binding
N
Motor
IQ
coiled
coil
C
Lipid-binding
mC-ATM2
mC-ATM2ΔLB
mC-ATM2CT
unclear
Actin-binding
Lipid-binding (LB)
tag
NT
SH3
Motor
IQ
CT
1
1220
1177
972
B
Kymograph
mTalin-YFP
mC
mTalin-YFP
mC-ATM2
mTalin-YFP
mC-ATM2ΔLB
mTalin-YFP
mC-ATM2CT
Distance from tip
Time
Merge
mC
YFP
C
Intensity ratio PM/cytosol
mC-ATM2
mC-ATM2ΔLB
D
Tip width [µm]
E
Tip actin occupancy [%]
F
Mean actin lifetime [min]
mC
mC-ATM2
mC-ATM2ΔLB
mC-ATM2CT

Figure 2

Figure 2. Overexpression of ATM2 stabilizes actin dynamics and induces tip swelling morphology in pollen tube cells.

Distribution and motility of the actin cytoskeleton were monitored by laser-scanning confocal microscopy (LSM) in tobacco (*N. tabacum*) pollen tubes coexpressing the actin marker, mTalin-YFP, with either an mCherry (mC)-control, or with mC-tagged variants of ATM2, including full length ATM2 (mC-ATM2), an ATM2 variant lacking the C-terminal lipid-binding region (mC-ATM2$_{\Delta LB}$), or an ATM2 variant lacking N-terminal actin-binding and protein-interaction regions (mC-ATM2$_{CT}$). Expression was driven by a pLat52 promoter.

(**A**) Schematic representation of the ATM2 protein (left) and of the mC-fusions of ATM2 variants used (right panel). Numbers indicate ATM2 residue positions. C, C-terminus; CT, C-terminal domain; IQ, calmodulin-binding IQ-motif-domain; Motor, motor-ATPase domain; N, N-terminus; NT, N-terminal domain; SH3, SRC-homology 3-domain

(**B**) To capture actin dynamics, Z-stacks (2 µm steps) were acquired in 10 s intervals over 5 min. Left column, representative maximum intensity projections of merged mTalin-YFP and mCherry fluorescence channels. Mid and right column, separate Z-projection images of the YFP channel (mTalin) or the mCherry channel (control and ATM2 variants), respectively. Arrowheads, Locally increased mTalin-YFP signal at the plasma membrane. Scale bars, 10 µm. Right panels, Kymographs extracted from the pollen tube tip regions. Stabilized actin filaments are represented by horizontal lines.

(**C**) Degree of plasma membrane association of mC-ATM2 or the lipid-binding deficient mC-ATM2$_{\Delta LB}$ variant according to the fluorescence intensity ratio of mC signals at the plasma membrane vs. cytosol, as indicated. Data represent observations from 12 cells (mC-ATM2) or 13 cells (mC-ATM2$_{\Delta LB}$), respectively.

(**D-F**) Pollen tube cells coexpressing the actin marker mTalin-YFP with an mC-control, mC-ATM2, with mC-ATM2$_{\Delta LB}$, or with mC-ATM2$_{CT}$ were analyzed for cell morphology (**D**), actin occupancy in the cell apex (**E**), or for mean actin lifetime (**F**).

(**D**) Pollen tube tip width (in µm) determined from brightfield images using Fiji. Data represent observations from 29 cells (mC); 18 cells (mC-ATM2); 13 cells (mC-ATM2$_{\Delta LB}$); or 14 cells (mC-ATM2$_{CT}$), respectively.

(**E**) The tip actin occupancy quantified as the relative area covered by mTalin-YFP signal at the pollen tube tip. Data represent observations from 25 cells (mC); 18 cells (mC-ATM2); 16 cells (mC-ATM2$_{\Delta LB}$); or 14 cells (mC-ATM2$_{CT}$), respectively.

(**F**) Mean lifetime (in min) of mTalin-labeled actin filaments, calculated from kymographs. Data represent observations from 20 cells (mC); 18 cells (mC-ATM2); 13 cells (mC-ATM2$_{\Delta LB}$); or 14 cells (mC-ATM2$_{CT}$), respectively.

Data in (**C-F**) represents 3-4 independent experiments. Statistical differences were assessed by one-way ANOVA followed by Tukey's post-hoc test; letters denote categories of values exhibiting statistical significant differences ($p < 0.05$).

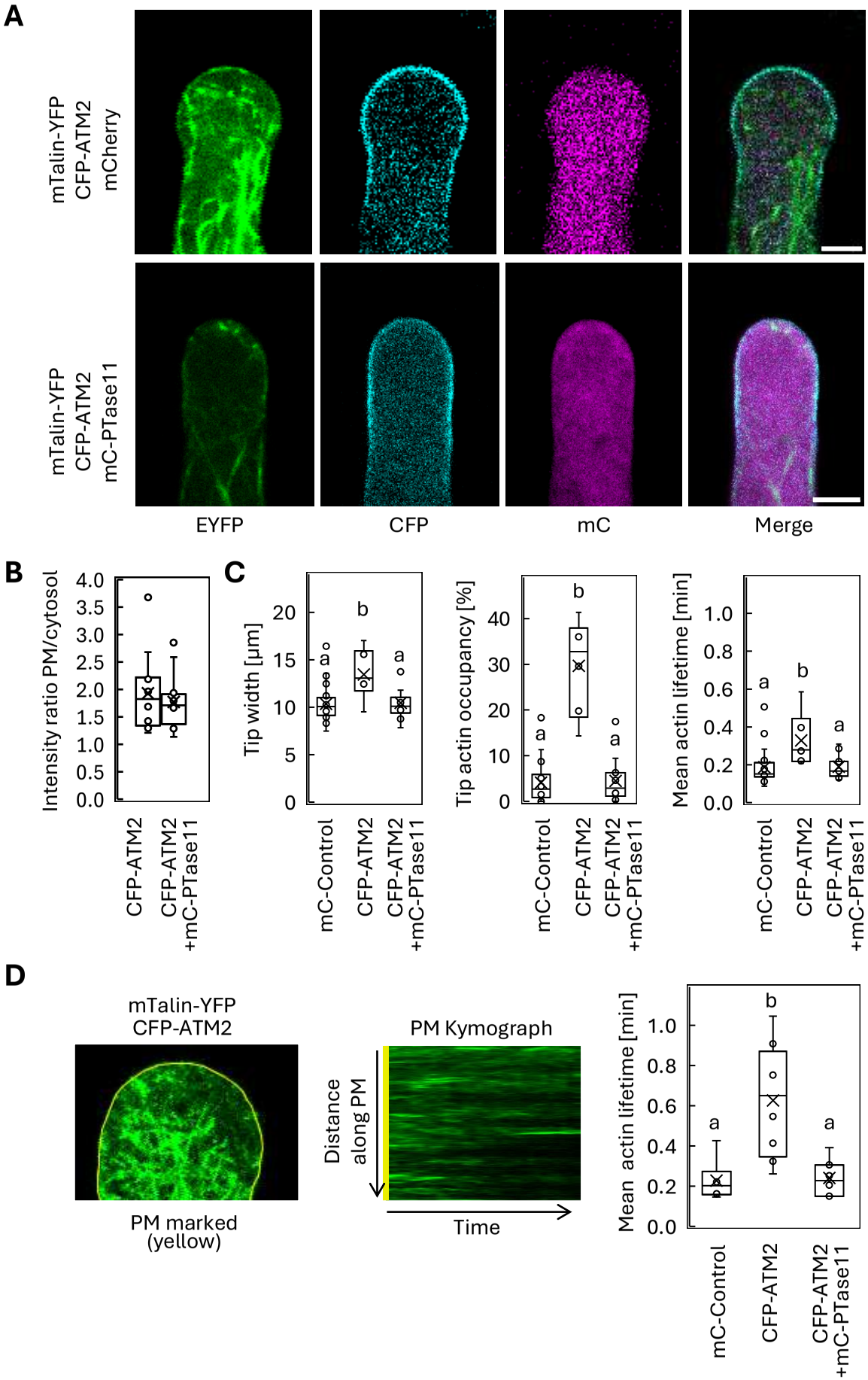

A
mTalin-YFP
CFP-ATM2
mCherry
mTalin-YFP
CFP-ATM2
mC-PTase11
EYFP
CFP
mC
Merge
B
Intensity ratio PM/cytosol
CFP-ATM2
CFP-ATM2 +mC-PTase11
C
Tip width [µm]
Tip actin occupancy [%]
Mean actin lifetime [min]
mC-Control
CFP-ATM2
CFP-ATM2 +mC-PTase11
D
mTalin-YFP
CFP-ATM2
PM marked (yellow)
PM Kymograph
Distance along PM
Time
Mean actin lifetime [min]
mC-Control
CFP-ATM2
CFP-ATM2 +mC-PTase11

Figure 3

Figure 3. Artificial PtdIns(4,5)P_2 depletion in the plasma membrane abolishes ATM2 effects on actin dynamics.

Effects of altered plasma membrane PtdIns(4,5)P_2 abundance on the function of ATM2 were studied for pollen tubes coexpressing CFP-ATM2 either with an mC control, or with the PtdIns(4,5)P_2-specific 5-phosphatase, mC-AtPTase11, an enzyme converting PtdIns(4,5)P_2 to PtdIns4P. Transgenic pollen tube cells were then analyzed for cell morphology, tip actin occupancy or mean actin lifetime. Expression was driven by a Lat52 promoter.

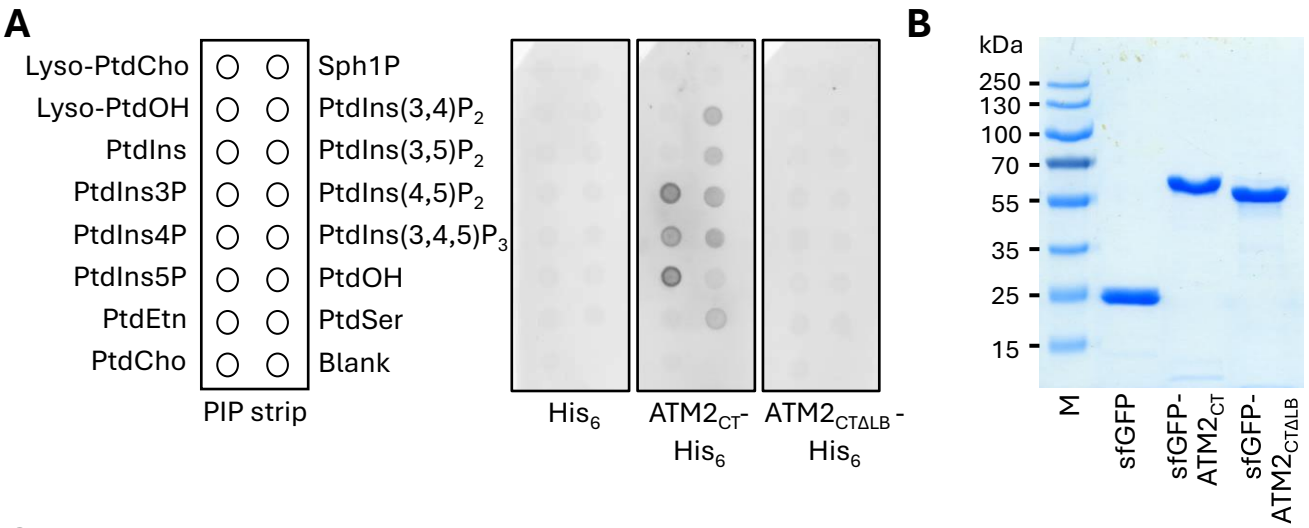
(**A**) Representative fluorescence images of pollen tubes coexpressing mTalin-YFP with CFP-ATM2 and either an mC control (upper panels) or with mC-AtPTase11 (lower panels), as indicated. Individual fluorescence channels and merged images, as indicated. Scale bars, 5 µm.

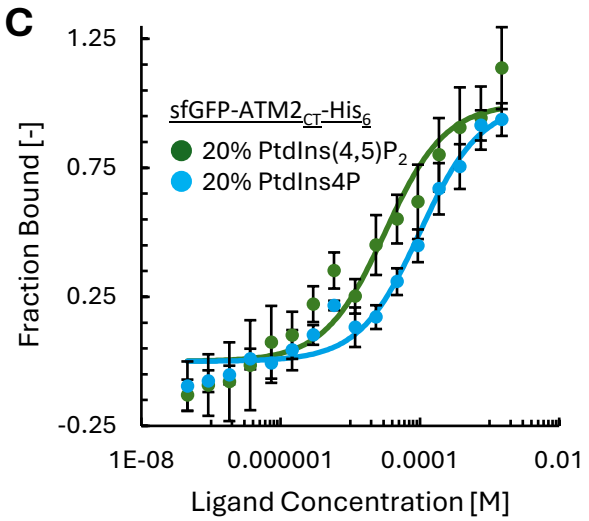
(**B**) Degree of plasma membrane association of CFP-ATM2 in control cells coexpressing mC or in cells coexpressing mC-PTase11 according to the fluorescence intensity ratio of mC signals at the plasma membrane vs. cytosol. Data represent observations from 12 cells (mC) or 12 cells (mC-PTase11), respectively.

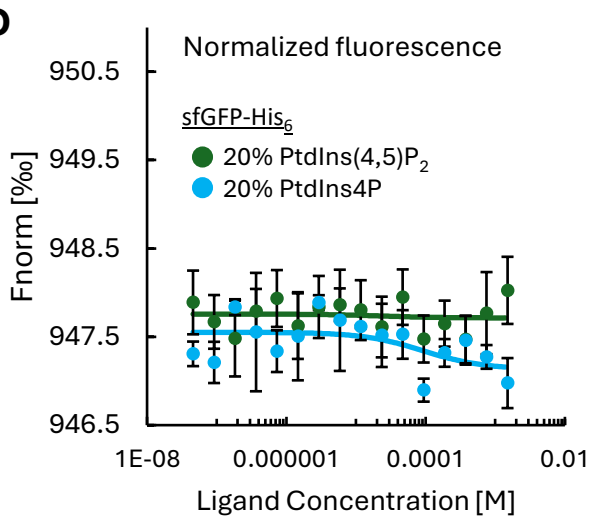
(**C**) Pollen tube tip with in µm (left panel), apical actin occupancy (mid panel), or mean actin lifetime in min (right panel) of mTalin-YFP-labeled actin filaments, as indicated. Data represent observations from 20-29 cells (mC-control); 6 cells (CFP-ATM2 plus mC); or 15 cells (mC-AtPTase11), respectively. Data were collected from at least three independent experiments.

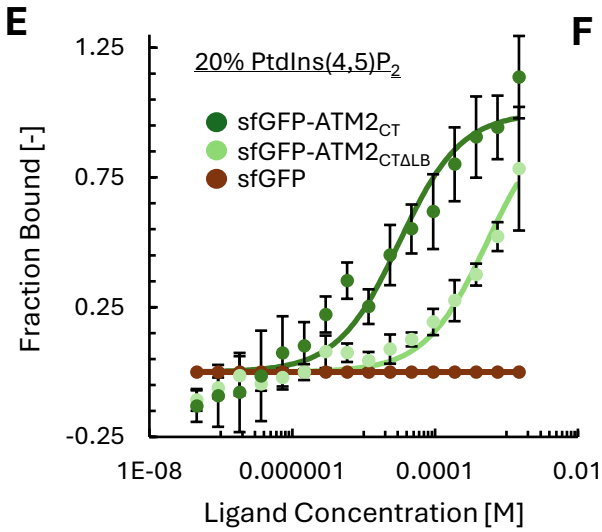
(**D**) The mean actin lifetime of plasma membrane-proximal actin decorated by mTalin-YFP was recorded by acquiring kymographs along the plasma membrane periphery of the cell apex (yellow line). Images (left panels) are illustrating the analysis done. Right panel, Plasma membrane-peripheral mean actin lifetime for control pollen tubes expressing only mC, or for cells coexpressing CFP-ATM2 either with an mC control, or with mC-AtPTase11, as indicated. Data represent observations from 6 cells (mC-control); 8 cells (CFP-ATM2 plus mC); or 7 cells (mC-AtPTase11), respectively. Data were collected from at least three independent experiments.

Statistical differences were assessed by one-way ANOVA followed by Tukey's post-hoc test; letters denote categories of values exhibiting statistical significant differences ($p < 0.05$).









F

Protein	Liposome	K_D	relative affinity
sfGFP-ATM2$_{CT}$-His$_6$	80 % DOPC 20 % PtdIns4P	99 µM	0.313
	80 % DOPC 20 % PtdIns(4,5)P_2	32 µM	1
sfGFP-ATM2$_{CTΔLB}$-His$_6$	80 % DOPC 20 % PtdIns(4,5)P_2	534 µM	0.059

Figure 4

Figure 4. Lipid-binding features of recombinant C-terminal ATM2 fragments.

Lipid binding of the polybasic C-terminal region of ATM2 was revisited by biochemical analysis, including quantitative MST-analysis. ATM2-variants representing the C-terminal region of ATM2 ($ATM2_{CT}$, residues 972-1220,) or the derived lipid binding-deficient variant $ATM2_{CT\Delta LB}$ (residues 972-1177) were recombinantly expressed as fusions to C-terminal His_6-tags, enriched, and used for *in vitro* protein-lipid interaction tests. For MST-analysis, protein were additionally fused to N-terminal superfolder (sf)GFP-tags. Enriched sfGFP or MBP alone were used as negative controls, respectively.

(**A**) Protein-lipid overlay assay for binding of a MBP-His_6 control, $ATM2_{CT}$-His_6 or $ATM2_{CT\Delta LB}$-His_6 to phospholipids (10 nmol) using commercial PIP strips (Echelon Biosciences Inc.). Images of the developed protein-lipid overlay blots are representative for three experiments.

(**B**) Exemplary Coomassie blue-stained SDS-PAGE gel of enriched recombinant sfGFP-fusions used for lipid-binding tests by MST, as indicated. Deduced fragment masses: sfGFP-His_6, 28.5 kDa; sfGFP-$ATM2_{CT}$-His_6, 57.6 kDa; sfGFP-$ATM2_{CT\Delta LB}$-His_6, 52.4 kDa.

(**C**) MST-analysis of the binding of enriched sfGFP–$ATM2_{CT}$-His_6 to DOPC-liposomes containing 20 mol% PtdIns(4,5)P_2 (green) or 20 mol% PtdIns4P (blue). Binding curves depict the fraction of bound protein plotted versus the logarithmic ligand concentration. Proteins were incubated at an approx. concentration of 40 nM with liposomes serially diluted from 45.78 nM - 3 mM total lipid over 16 dilution steps. The MST-on time was 2.5 s; data were fitted with the KD-fit model. Each point represents four independent measurements; error bars indicate standard deviation.

(**D**) MST control-measurements with enriched sfGFP-His_6 and DOPC-liposomes containing 20 mol% PtdIns(4,5)P_2 (green) or 20 mol% PtdIns4P (blue). As no binding was detected for sfGFP-His_6, data is represented as Fnorm in ‰ against the logarithmic ligand concentration.

(**E**) MST-analysis comparing the binding of enriched $ATM2_{CT}$ (dark green), $ATM2_{CT\Delta LB}$-His_6 (light green) or sfGFP-His_6 (brown) to DOPC-liposomes containing 20 mol% PtdIns(4,5)P_2. MST-on time was 2.5 s and data were fitted using the KD-fit model. Each data point represents four independent measurements with error bars indicating standard deviation. $ATM2_{CT}$ data are same as in (**C**).

(**F**) KD values representing binding affinities for measurements presented in (**C**) or (**E**). Signal to noise ratios (not shown) were above 5, reflecting reliable binding measurements. Relative affinities are given for binding to PtdIns(4,5)P_2-containing liposomes as a reference (right column).

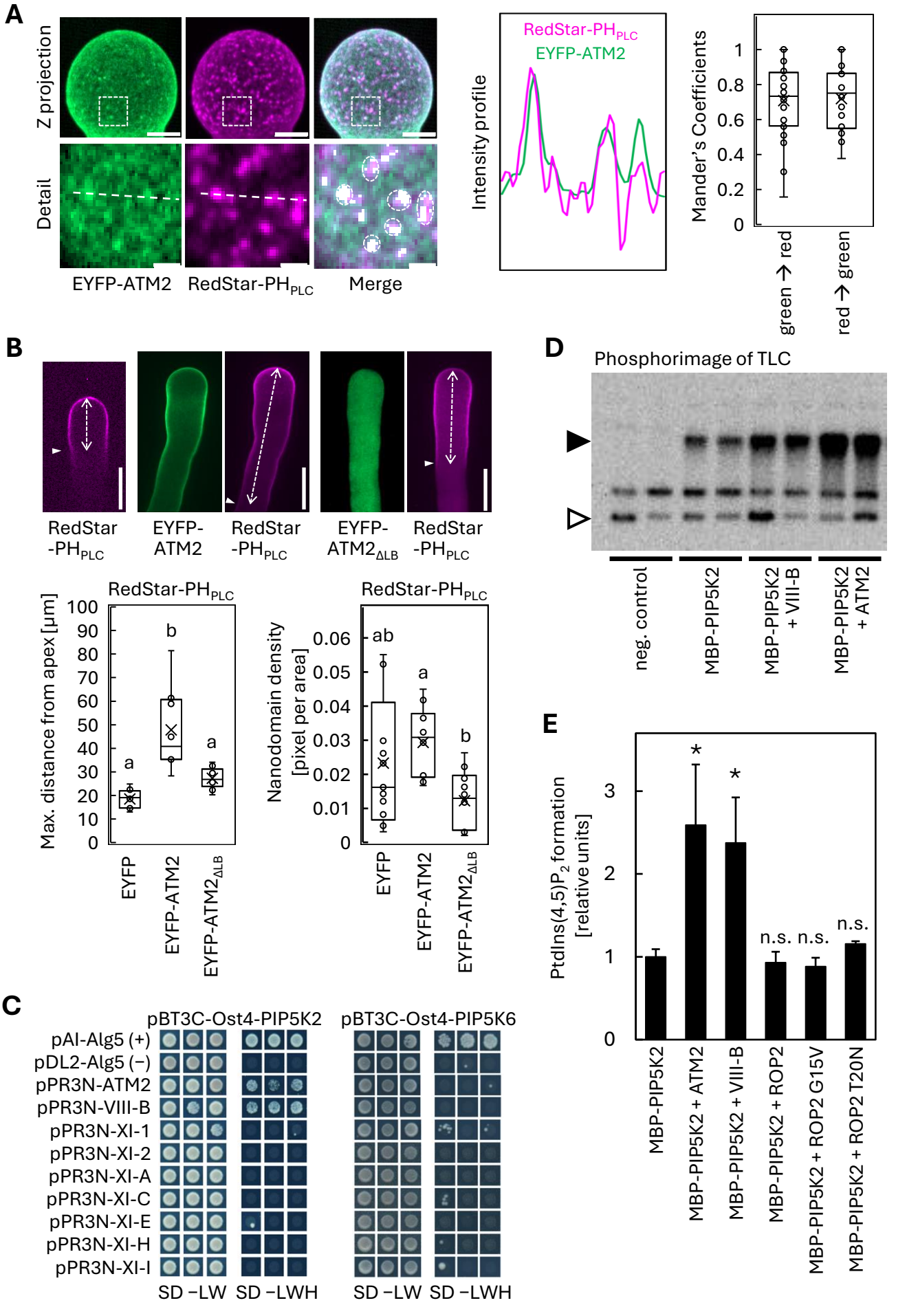

A
Z projection
Detail
EYFP-ATM2
RedStar-PHPLC
Merge
RedStar-PHPLC
EYFP-ATM2
Intensity profile
Mander's Coefficients
green → red
red → green
B
RedStar -PHPLC
EYFP-ATM2
RedStar -PHPLC
EYFP-ATM2ΔLB
RedStar -PHPLC
RedStar-PHPLC
Max. distance from apex [µm]
EYFP
EYFP-ATM2
EYFP-ATM2ΔLB
Nanodomain density [pixel per area]
C
pBT3C-Ost4-PIP5K2
pBT3C-Ost4-PIP5K6
pAI-Alg5 (+)
pDL2-Alg5 (−)
pPR3N-ATM2
pPR3N-VIII-B
pPR3N-XI-1
pPR3N-XI-2
pPR3N-XI-A
pPR3N-XI-C
pPR3N-XI-E
pPR3N-XI-H
pPR3N-XI-I
SD −LW
SD −LWH
SD −LW
SD −LWH
D
Phosphorimage of TLC
neg. control
MBP-PIP5K2
MBP-PIP5K2 + VIII-B
MBP-PIP5K2 + ATM2
E
PtdIns(4,5)P2 formation [relative units]
n.s.
n.s.
n.s.
MBP-PIP5K2
MBP-PIP5K2 + ATM2
MBP-PIP5K2 + VIII-B
MBP-PIP5K2 + ROP2
MBP-PIP5K2 + ROP2 G15V
MBP-PIP5K2 + ROP2 T20N

Figure 5

Figure 5. ATM2-EYFP colocalizes with RedStar-PH_{PLC} in plasma membrane nanodomains and promotes PtdIns(4,5)P_2 formation by PIP5K2 *in vivo* and *in vitro*.

The functional interplay of ATM2 with PtdIns(4,5)P_2 or PIP5K2 was analyzed in more detail by *in vivo* and *in vitro* experiments.

(**A**) Fluorescence distribution of ATM2-EYFP and the coexpressed PtdIns(4,5)P_2 biosensor, RedStar-PH_{PLC} in tobacco pollen tubes, visualized by spinning disc microscopy (SD). Images represent maximum intensity projections from z-stacks acquired in 0.3 µm slices. Upper panels, 3D projections of the EYFP channel (left), RedStar channel (mid), and the merged image (right). Scale bar, 5 µm. Lower panels, magnified regions of interest (white boxes). Scale bars, 1 µm. Right panels, Fluorescence intensity plots for the EYFP and RedStar channels, recorded along the dashed line. Mander's colocalization coefficients were calculated for fluorescent nanodomains in red → green and in green → red directions, as indicated.

(**B**) Spatial extent of the subapical plasma membrane domain decorated by RedStar-PH_{PLC} upon coexpression with a EYFP-control (left panel), with ATM2-EYFP (mid panel), or with $ATM2_{\Delta LB}$-EYFP (right panel), as indicated. Upper panels show representative images, respectively. Please note the loss of plasma membrane association for $ATM2_{\Delta LB}$-EYFP. Arrows indicate the extent of the RedStar-PH_{PLC}-labeled membrane domain as maximum didtance from apex. Lower panels, Spatial extent of the plasma membrane domain labeled by RedStar-PH_{PLC} upon coexpression with the EYFP-control, with ATM2-EYFP, or with $ATM2_{\Delta LB}$-EYFP, as indicated (left). The area density of punctate signals decorated by RedStar-PH_{PLC} was analyzed for pollen tubes expressing the EYFP-control, ATM2-EYFP, or $ATM2_{\Delta LB}$-EYFP, as indicated (right). Data represent observations from 8 cells (EYFP-control); 14 cells (ATM2-EYFP); or 9 cells (ATM2-$EYFP_{\Delta LB}$), respectively. Statistical differences were assessed by one-way ANOVA followed by Tukey's post-hoc test; letters denote categories of values exhibiting statistical significant differences ($p < 0.05$).

(**C**) Yeast-two-hybrid analysis using PIP5K2 or PIP5K6, respectively, as bait proteins against selected myosin isoforms, including the pollen-specific class VIII myosins ATM2 or VIIIB, and various class XI myosins, as indicated. Left panels, interaction tests with PIP5K2 as a bait; right panels, interactions tests with PIP5K6 as a bait. Yeast growth on non-selective SD–LW medium confirmed correct transformation, while growth on selective SD–LWH medium indicated positive interactions. Results are representative for three independent biological replicates, each performed in triplicates.

(**D**) Enriched recombinant MBP-PIP5K2 fusion protein expressed in *E. coli* was tested for *in vitro* catalytic activity, converting PtdIns4P to PtdIns(4,5)P_2 in the presence of [γ-^{32}P]ATP. Formation of radiolabeled PtdIns(4,5)P_2 was monitored by phosphormaging after chromatographic separation of the reaction products. Assays were performed with *E. coli* extract as a negative control, with MBP-PIP5K2 alone, or upon coincubation of MBP-PIP5K2 with enriched recombinant C-terminal fragments of the class VIII-myosins, VIII-B or ATM2, as indicated. The image shows a representative phosphorimage. The experiment was performed five times with similar results.

(**E**) Quantification of PtdIns(4,5)P_2 production from assays shown in (**D**), reported in relative units. Additional controls include coincubation of MBP-PIP5K2 with the small GTPase ROP2 (a PtdIns(4,5)P_2-binding protein) and its constitutively active (G15V) or dominant-negative (T20N) variants, as indicated. Asterisks indicate statistical differences from the MBP-PIP5K2 control, according to a Student's *t*-test ($p < 0.05$). n.s., not significant.

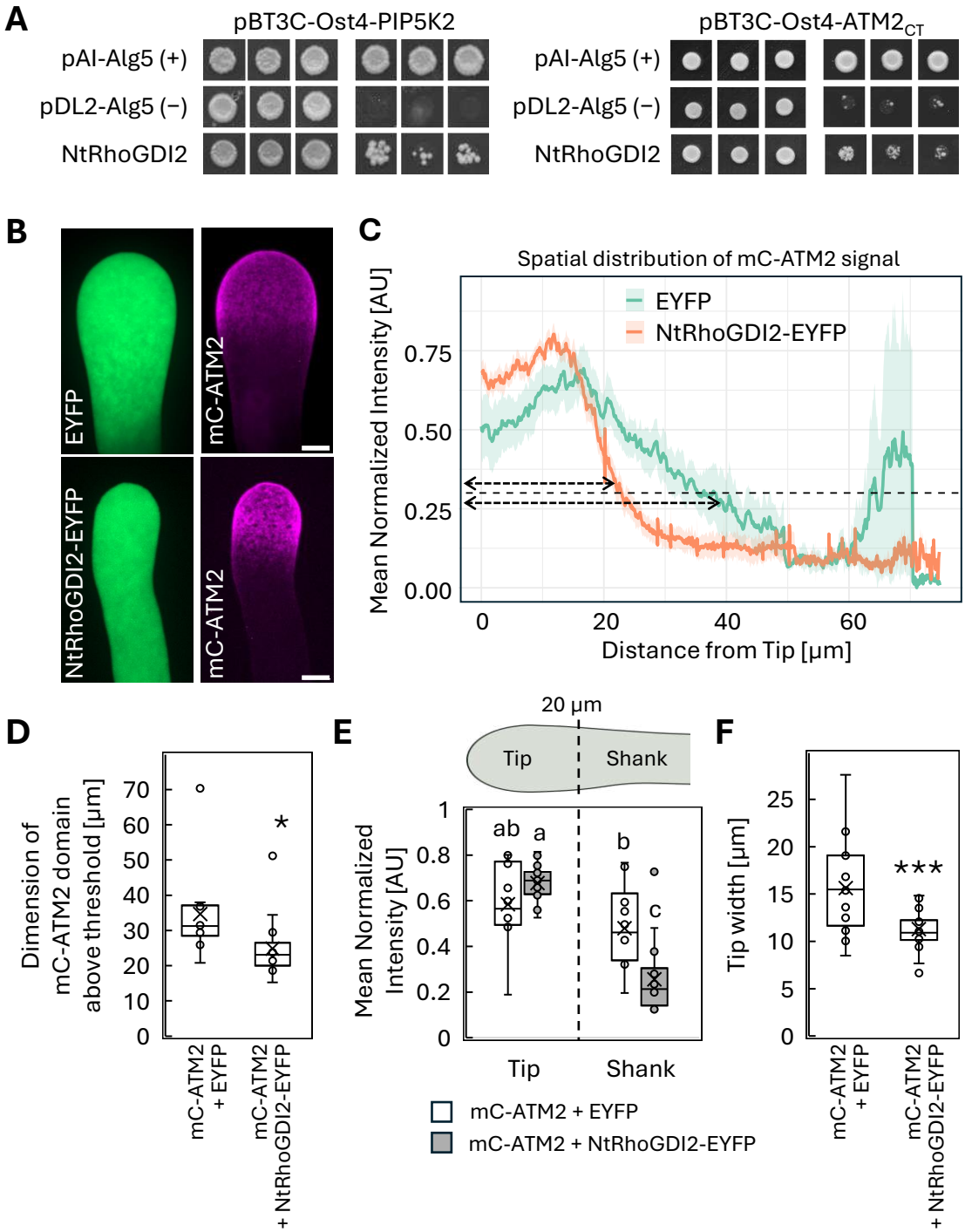

A
pBT3C-Ost4-PIP5K2
pBT3C-Ost4-ATM2CT
pAI-Alg5 (+)
pDL2-Alg5 (−)
NtRhoGDI2
B
EYFP
mC-ATM2
NtRhoGDI2-EYFP
mC-ATM2
C
Spatial distribution of mC-ATM2 signal
EYFP
NtRhoGDI2-EYFP
Mean Normalized Intensity [AU]
0.00
0.25
0.50
0.75
0
20
40
60
Distance from Tip [µm]
D
Dimension of mC-ATM2 domain above threshold [µm]
0
10
20
30
40
50
60
70
*
mC-ATM2 + EYFP
mC-ATM2 + NtRhoGDI2-EYFP
E
20 µm
Tip
Shank
Mean Normalized Intensity [AU]
0
0.2
0.4
0.6
0.8
1
ab
a
b
c
Tip
Shank
mC-ATM2 + EYFP
mC-ATM2 + NtRhoGDI2-EYFP
F
Tip width [µm]
0
5
10
15
20
25
***
mC-ATM2 + EYFP
mC-ATM2 + NtRhoGDI2-EYFP

Figure 6

Figure 6. Effects of ATM2 are influenced by coexpression of NtRhoGDI2.

The guanine-nucleotide dissociation inhibitor, NtRhoGDI2, was previously shown to counteract PIP5K2/PtdIns(4,5)P_2-dependent stabilization of actin dynamics in pollen tubes. The influence of NtRhoGDI2 on ATM2-mediated effects was analyzed by protein-protein interaction studies, by coexpression of fluorescent protein fusions in tobacco pollen tubes, and by assessing pollen tube cell morphology.

(**A**) Yeast-two-hybrid analysis using PIP5K2 or ATM2, respectively, as bait proteins against NtRhoGDI2. Left, interaction tests with PIP5K2 as a bait; right, interactions tests with ATM2 as a bait. Yeast growth on non-selective SD–LW medium confirmed correct transformation, while growth on selective SD–LWH medium indicated positive interactions. Results are representative for three independent biological replicates, each performed in triplicates.

(**B**) Representative confocal images of tobacco pollen tubes coexpressing mC-ATM2 with either EYFP (top) or with NtRhoGDI2-EYFP (bottom), as indicated. Scale bars, 5 µm.

(**C**) Spatial distribution of mC-ATM2 mean normalized fluorescence intensity (±SEM) along the plasma membrane, plotted as mean normalized intensity (AU) against the distance from the apex (µm) for mC-ATM2 coexpressed with EYFP (green) or with NtRhoGDI2-EYFP (orange). The dashed line indicates the threshold of 0.25 intensity units used for domain signal length estimation. Data represent observations from 10 cells (EYFP) or 18 cells (NtRhoGDI2-EYFP), respectively, from two independent experiments.

(**D**) Dimension of the plasma membrane domain decorated by mC-ATM2 above the 0.25 threshold in pollen tubes coexpressing mC-ATM2 with either EYFP or with NtRhoGDI2-EYFP, as indicated. Data represent 2-3 independent experiments. The asterisk indicates a significantly difference according to a Student's *t*-test ($p < 0.05$).

(**E**) Mean normalized fluorescence intensity of mC-ATM2 coexpressed with EYFP (white) or with NtRhoGDI2-EYFP (grey), in the tip (0-20 µm distance from apex) or shank regions (20-40 µm distance from apex) of the pollen tube cells. Data represent 2-3 independent experiments. Statistical differences were determined by one-way ANOVA followed by Tukey's post-hoc test; letters denote categories of values exhibiting statistical significant differences ($p < 0.05$).

(**F**) Pollen tube tip with in µm of pollen tubes coexpressing ATM2-MC with EYFP or with NtRhoGDI2-EYFP, as indicated. Data represents two independent experiments. The asterisk indicates a significantly difference according to a Student's *t*-test ($p < 0.001$).

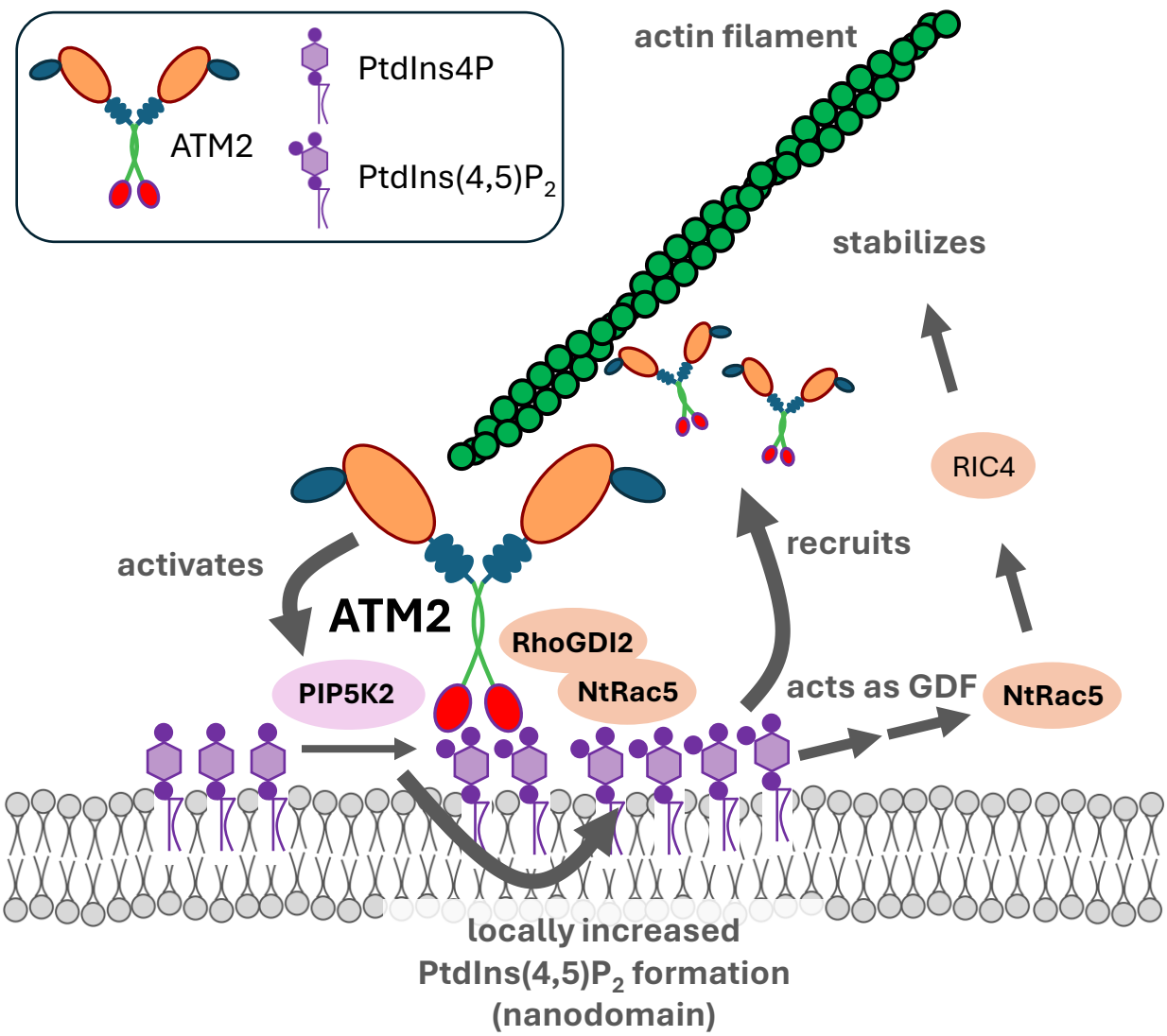
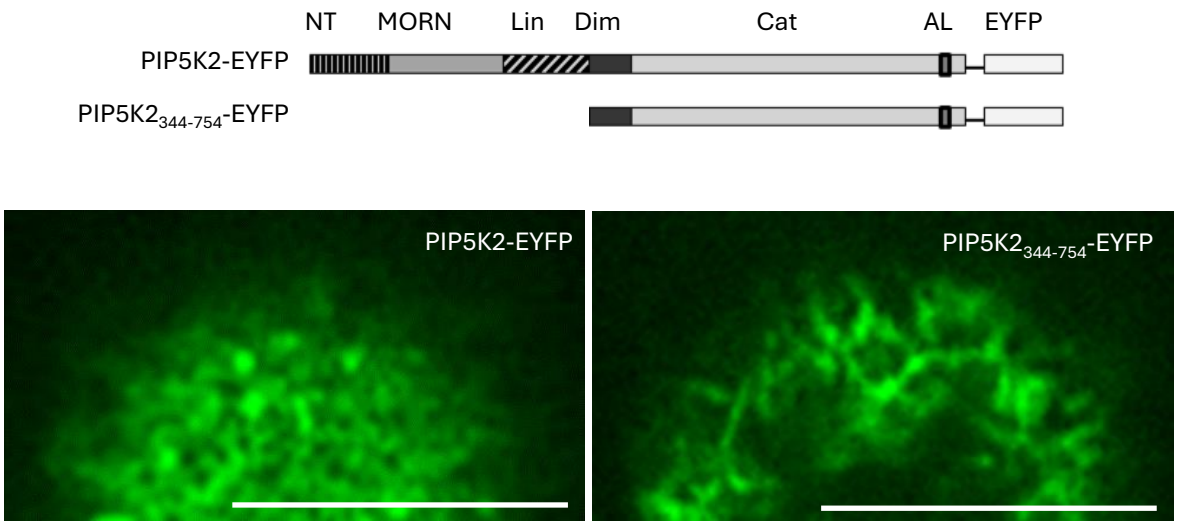


Figure 7. Simplified schematic of ATM2-mediated activation of PIP5K2, locally potentiating PtdIns(4,5)P_2 production at the actin-plasma membrane interface.

The class VIII myosin ATM2 forms an interface between actin filaments and the plasma membrane by binding to anionic phospholipid headgroups and to actin filaments. ATM2 might at least transiently occur in complex with PIP5K2 and NtRhoGDI2. By binding to ATM2, catalytic activity of PIP5K2 is enhanced, thereby promoting PtdIns(4,5)P_2 formation at actin-plasma membrane contact sites. The locally increased abundance of PtdIns(4,5)P_2 acts as a positional signal for the recruitment of further ATM2 proteins, and acts as a GDF on NtRhoGDI2, mediating enhanced activation of Rac/ROP proteins, to facilitate actin stabilization. Alternative explanations are possible. GDF, guanine nucleotide displacement factor; PtdIns4P, phosphatidylinositol 4-phosphate; PtdIns(4,5)P_2, phosphatidylinositol 4,5-bisphosphate

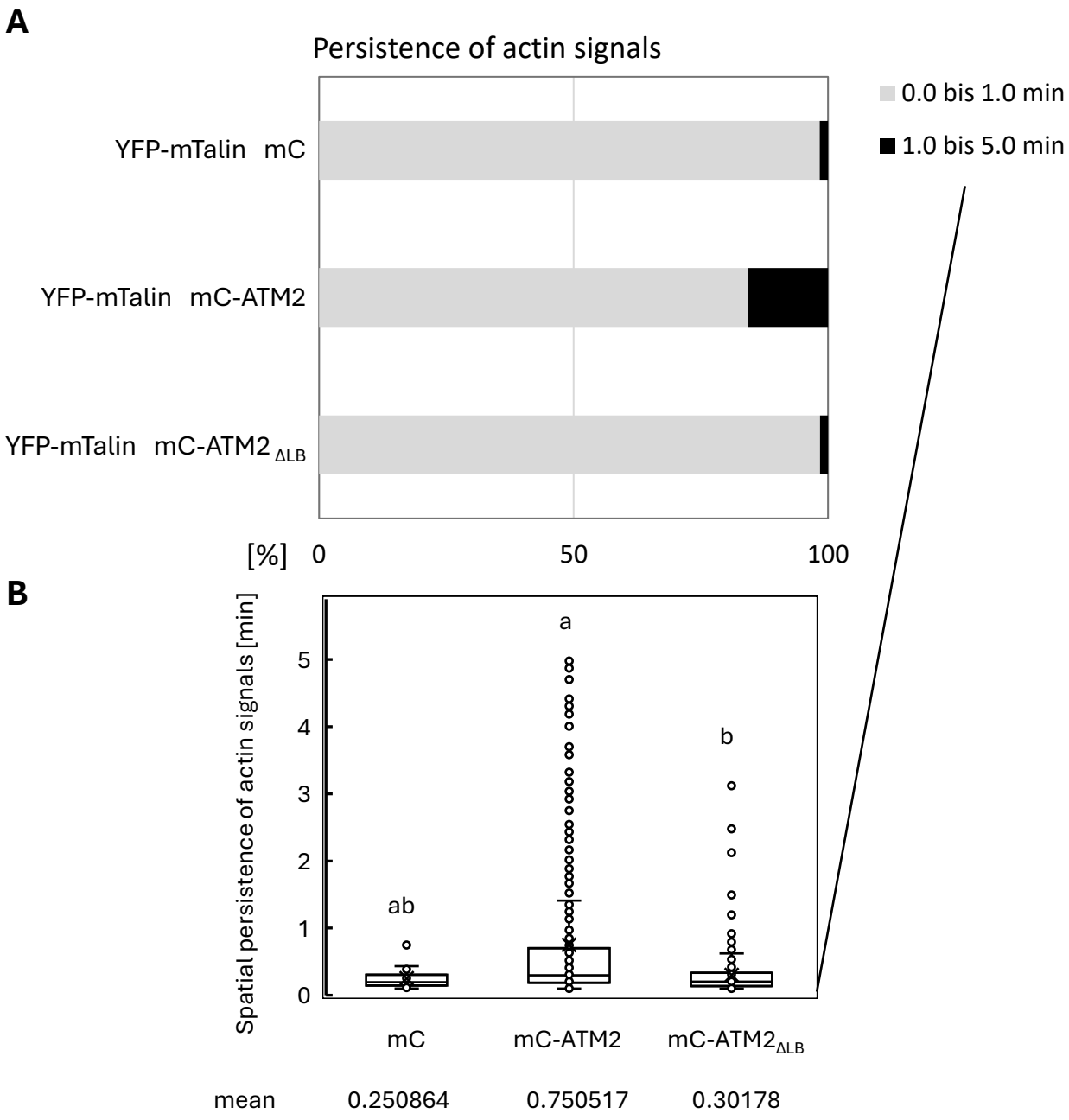


Supplemental Figure 1. Relaxed localization of AtPIP5K2$_{344-754}$-EYFP in a plasma membrane-peripheral network-like pattern in tobacco pollen tubes.

The fluorescence distribution of AtPIP5K2-EYFP or the N-terminally truncated AtPIP5K2$_{344-754}$-EYFP was analyzed by spinning disc microscopy upon transient expression in tobacco pollen tubes.

Top panel, Representation of the expressed EYFP fusion proteins. NT, N-terminal domain; MORN, membrane occupation and recognition nexus repeat domain; Lin, hypervariable linker region; Dim, dimerization domain; Cat, catalytic domain; AL, activation loop

Bottom panels, AtPIP5K2-EYFP displays dot-like plasma membrane association resembling nanodomains in the apex of a tobacco pollen tube (left). AtPIP5K2$_{344-754}$-EYFP decorates a plasma membrane-proximal filamentous network-pattern, possibly representing the cortical actin network. Images are representative for three independent experiments.

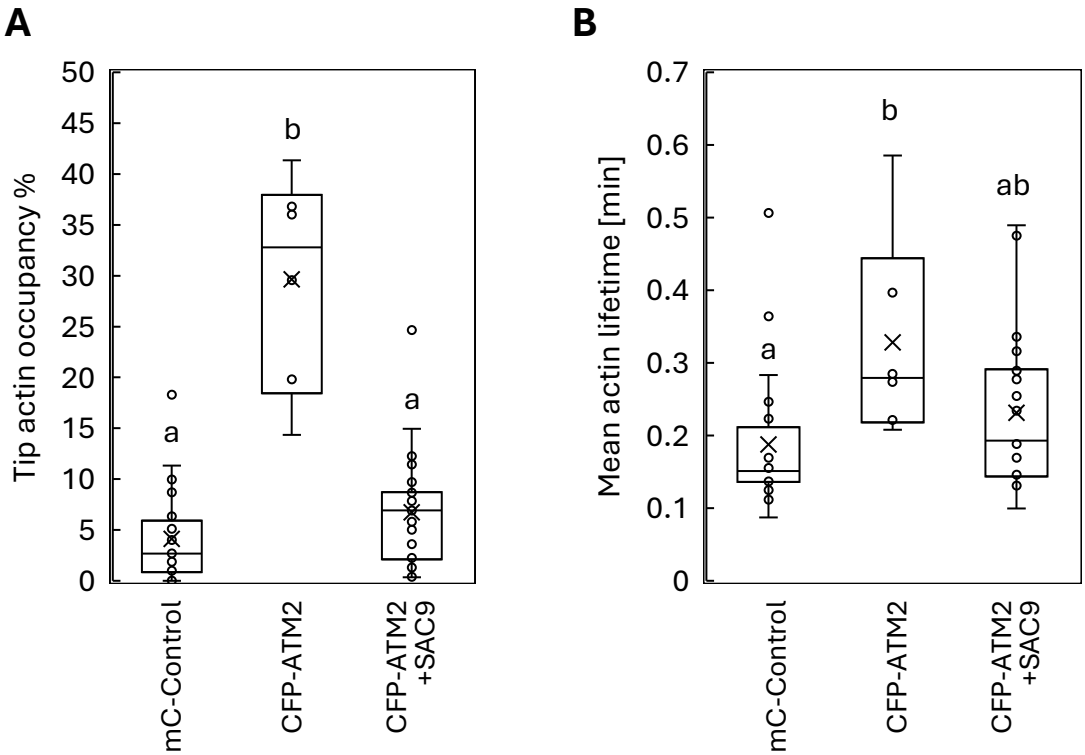


Supplemental Figure 2. Detailed analysis of mean actin lifetimes in pollen tube cells expressing an mC-control, mC-ATM2, or mC-ATM2$_{\Delta LB}$.

Data from the analysis of mean lifetimes of mTalin-labeled actin filaments were calculated from kymographs and analyzed for the proportion of filaments displaying low-mobility.

(**A**) Proportion of mTalin-YFP sigbals displaying a spatial persistence of 0 min - 1 min (grey, high mobility) or of 1 min - 5 min (black, low mobility).

(**B**) Exact number underlying the representation in (**A**). Data represent observations from 20 cells (mC); 18 cells (mC-ATM2); 13 cells (mC-ATM2$_{\Delta LB}$); or 14 cells (mC-ATM2$_{CT}$), respectively.



Supplemental Figure 3. Artificial PtdIns(4,5)P_2 depletion in the plasma membrane abolishes ATM2 effects on actin dynamics.

Effects of altered plasma membrane PtdIns(4,5)P_2 abundance on the function of ATM2 were studied for pollen tubes coexpressing CFP-ATM2 either with an mC control, or with the PtdIns(4,5)P_2-specific 5-phosphatase, SAC9, an enzyme converting PtdIns(4,5)P_2 to PtdIns4P. Transgenic pollen tube cells were then analyzed for cell morphology or mean actin lifetime. Expression was driven by a Lat52 promoter.

(**A**) Actin occupancy in the cell apex was determined for cells expressing fluorescent fusion proteins, as indicated. Data were collected from at least three independent experiments (mC-control, 25 cells; CFP-ATM2, 6 cells; SAC9, 25 cells).

(**B**) Mean actin lifetime of mTalin-YFP signals was recorded by acquiring kymographs. Data were collected from at least three independent experiments (mC-control, 20 cells; CFP-ATM2, 6 cells; SAC9, 25 cells).

Statistical differences were assessed by one-way ANOVA followed by Tukey's post-hoc test; letters denote categories of values exhibiting statistical significant differences ($p < 0.05$).